Annals of Glaciology

Article

Cite this article: Zhang X, Haapala J, Uotila P (2024). Capacity of a set of CMIP6 models to simulate Arctic sea ice drift. *Annals of Glaciology* **65**, e24, 1–19. https://doi.org/10.1017/aog.2024.25

Received: 7 November 2023
Revised: 10 July 2024
Accepted: 28 July 2024

Keywords:
sea ice; sea-ice dynamics; sea-ice modeling

Corresponding author:
Xinfang Zhang;
Email: xinfang.zhang@fmi.fi

Capacity of a set of CMIP6 models to simulate Arctic sea ice drift

Xinfang Zhang[1], Jari Haapala[1] and Petteri Uotila[2]

[1]Marine Research Unit, Finnish Meteorological Institute, Helsinki, Finland and [2]Institute for Atmospheric and Earth System Research/Physics, University of Helsinki, Helsinki, Finland

Abstract

Evaluating CMIP6 model performance helps to improve the prediction of future changes in Arctic sea ice. We analyze the seasonal cycles, distribution, and evolution of sea ice in different regions from 1979 to 2014. We compare the output from selected CMIP6 models with reference data for sea ice motion. We also discuss the correlations between sea ice motion(SIM) and sea ice thickness (SIT) in reference data, and how CMIP6 models explain them. We select EC-Earth3, ACCESS-CM2, BCC-CSM2-MR, MPI-ESM1-2-HR, and NorESM2-LM for CMIP6 study. We compare outputs with reference data: Sea ice extent (SIE) from NSIDC; SIT from PIOMAS; and SIM from the IABP buoy data. Analytical techniques include Theil-Sen and Ordinary least squares (OLS) regression. Most selected CMIP6 models have seasonal cycles of SIM lagging behind IABP observations by 1-2 month and overestimate central Arctic SIM magnitude, with MPI-ESM1-2-HR having the highest discrepancy and NorESM2-LM lowest. The models show better simulation of SIM in the ice melting season than in the growing season. Models perform worse at capturing regional differences in SIM evolution and are overly conservative when simulating the increasing trend in ice motion, especially in coastal Arctic seas during summer. There is significant negative correlation between SIT and SIM in October.

Introduction

The description of sea ice physics in global climate models has improved considerably since the 1970s (Hunke and Comeau, 2011; Mackie and others, 2020). In contrast to early-generation climate models that treated sea ice as a simple thermodynamic slab over the ocean, state-of-the-art models now resolve the halo-thermodynamics of snow and ice for several layers (Vancoppenolle and others, 2009). They calculate sub-grid scale ice thickness variations (Thorndike and others, 1975; Bitz and others, 2001), and apply rheology that takes into account the strong coupling of sea ice mass and momentum balance (Hibler, 1979).

So far, the validation studies of sea ice in the Coupled Model Inter-comparison Project phase 6 (CMIP6) have mainly concentrated on the variability and changes in the annual mean sea ice extent (SIE) and sea ice thickness (SIT), as well as on the spatial variations of these parameters in the Arctic (Notz and SIMIP community, 2020; Watts and others, 2021). On the other hand the sea ice simulated in CMIP5 was 1–2 m too thin (Voldoire and others, 2013), Notz and SIMIP community (2020) showed that CMIP6 produced good estimates for SIE and performed better in capturing the sensitivity of sea ice to forcing compared with both CMIP3 and CMIP5. Watts and others (2021) pointed out that CMIP6 simulated the seasonal cycle well for SIT and SIE, as well as the trend for SIT, yet they underestimated the decline of Arctic sea ice concentration (SIC) in March. CMIP6 simulations of sea ice volume (SIV) have larger spread and uncertainties in contrast sea ice area (SIA) (Lee and others, 2023). Xu and Li (2023) evaluated SIT simulation by 12 CMIP6 models with CICE components using satellite observations and PIOMAS reanalysis, and found that biases, variability, and trends of SIT vary in different sub-regions. Xu and Li (2023) indicated that the coupling of the CICE model with ocean and atmosphere models has vital importance to improving SIT simulation in CMIP.

To provide a complete assessment of the selected CMIP6 models' capacity to simulate sea ice conditions, it is essential to validate sea ice dynamics, which is a crucial factor affecting sea ice mass balance. The movement and circulation of sea ice play a crucial role in determining how long pack ice stays in the high Arctic. This reflects larger scale phenomena such as the Arctic Oscillation (AO) and the Dipole Anomaly (DA), as well as factors like the age of the sea ice (Rind and others, 2005) and its thickness distribution (Oikkonen and Haapala, 2011; Sumata and others, 2023). Furthermore, the variation in sea ice speed contributes to the overall mass of the ice by promoting new ice growth in leads and the redistribution of thin ice to pressure ridges in compression. Simultaneously, ice motion is to a great extent dependent on sea ice thickness and concentration. This relationship is not linear, and, in certain circumstances, very thick and compact pack ice can be nearly motionless despite considerable atmospheric or oceanic forcing (Leppäranta, 2010; Kwok and others, 2013). Docquier and others (2017) demonstrated that thinning of sea ice allows sea ice deformation and fracturing, leading to faster sea ice speed. When sea ice concentration is near 100% during the winter season, changes in thickness are the primary factor influencing sea ice motion.

https://doi.org/10.1017/aog.2024.25 Published online by Cambridge University Press

Meanwhile, in the warm season, ice concentration becomes the main driver (Olason and Notz, 2014).

Relatively few studies have evaluated CMIP models' skill in simulating sea ice drift. Crawford and others (2023) studied the bias in CMIP6 models of sea ice thickness and sea ice motion, comparing with PIOMAS in the Hudson Bay. They found that most CMIP6 models have a negative SIT bias, while the simulation of sea ice cyclonic circulation can be either too weak or too strong, depending on the model. For the Arctic Ocean, Rampal and others (2011) showed that CMIP3 models had substantial variations in modeled sea ice speed, with that none of them showing an increasing trend in ice drift similar to that observed trend. They concluded that this discrepancy was due to the weak coupling between sea ice mass and momentum in the CMIP3 models. CMIP5 models generally estimated sea ice dynamics well, specifically in a realistic simulation of transpolar drift and the Beaufort gyre circulation patterns (Chevallier and Salas y Melia, 2011). Furthermore, (Uotila and others, 2013) showed that during March the ACCESS model from CMIP5 simulated Arctic sea ice drifting patterns well; however in September it failed to simulate the transpolar ice drifting component. In the Southern Ocean, Schroeter and others (2018) observed that, within CMIP5, those models which had small sea ice motion magnitudes were dominated by thermodynamic processes, while those exhibiting substantial sea ice motion were attributed to the combined influences of dynamic and thermodynamic processes. Uotila and others (2013) identified ice velocity differences between CMIP5 models, and reasoned that this could be due to differences in the strength of coastal currents or differences in wind forcing. However, an updated analysis using CMIP6 models is needed.

In this study, we focus on evaluating the selected CMIP6 models' ability to simulate sea ice drift in the Arctic Ocean. Since changes in sea ice drift are expected to be related to sea ice mass balance, we also provide an analysis of climate models' capacity to simulate regional, seasonal, and inter-annual variations in ice thickness and extent. Finally, we examine the relationship between the sea ice state and sea ice dynamics among the selected models.

Data availability and method

Validation data

Sea ice concentration

Sea ice concentration and its corresponding grid cell area in the Arctic region are based on the National Snow and Ice Data Center (NSIDC) gridded monthly sea ice extent and concentration dataset (Walsh and others, 2017). These satellite observations cover the period from January 1979 to December 2014 with spatial resolution of $0.25^\circ \times 0.25^\circ$ in a latitude–longitude grid.

Sea ice thickness

Due to significant uncertainties in satellite-derived sea ice thickness (Gerland and others, 2019), we rely on the PIOMAS model data available at the Polar Science Center (Schweiger, 2011). PIOMAS (Pan-Arctic Ice Ocean Modeling and Assimilation System) assimilates observations into numerical models to provide an estimation of the variation of sea ice volume over decades. The model has been extensively validated through comparisons with observations from US-Navy submarines, oceanographic moorings, and satellites. The data covers the period from January 1979 to December 2021 with a monthly time resolution. Spatial coverage is 45° N–90° N and the typical grid cell size is 25 km × 42 km on average. Despite the uncertainties that exist in PIOMAS, it has the advantage of including summer data and having a longer record compared to other sources.

Sea ice motion

For our sea-ice motion study, we are utilizing the dataset from the International Arctic Buoy Programme (IABP) (Rigor, 2017). The distribution buoy density vary from year to year, with an overall increase in buoy deployments over time. In this study, we cover the latitudes from 50° N–90° N and years from 1979–2021. We calculate daily mean sea ice motion based on 12 hourly original buoy data. Different types of positioning systems on the buoys introduce uncertainties in buoy locations, ranging from 100 m to 300 m (Thomas, 1999). In a study by Rigor and others (2002), the error of monthly ice velocity calculated based on IABP buoy data was estimated to be less than or equal to 0.02 cm/s, taking into account a positioning error with an upper limit of 300 m for the Argos system. In Rampal and others (2009), cubic interpolation was used to regularize the IABP buoy positions. This result in sea ice motion uncertainties of 1.3–3 cm/s in 3 h interval data (or 0.054–0.125 cm/s in the monthly average).

For our SIT-SIM correlation study, we also introduced the NCEP-NCAR version of PIOMAS sea ice velocity data, to be consistent with PIOMAS SIT data. The temporal resolution is daily and we chose to focus on the central Arctic area 80° N–90° N. The temporal coverage is from 1979 to 2014. PIOMAS ice velocity data can be retrieved at https://pscfiles.apl.washington.edu/zhang/PIOMAS/data/v2.1/other/.

CMIP6

The CMIP6 (Coupled Model Inter-comparison Project phase 6) data is available at Earth System Grid Federation (ESGF, 2022). In our study, we rely on the model selection criteria outlined in Notz and SIMIP community (2020) to choose the most suitable CMIP6 models. Notz and SIMIP community (2020) evaluated CMIP6 model performance by comparing simulated SIE with observational data. Models falling within a range of ±2 standard deviations were considered plausible simulations. In addition, (Notz and SIMIP community, 2020) conducted sensitivity studies on SIE in response to CO2 emissions and global mean surface temperature (GMST) changes, identifying 13 models with plausible sensitivities.

We select the ACCESS-CM2, BCC-CSM2-MR, MPI-ESM1-2-HR, and NorESM2-LM models from the 13 models for the following reasons: First, they are identified by Notz and SIMIP community (2020) as good performers; Second, hey have all necessary sea ice parameters (monthly sea ice concentration, monthly sea ice thickness and daily sea ice motion); Third, they have at least three ensemble members. Fourth, they have a 'historical' experiment. The EC-Earth3 model is also selected because the Finnish Meteorological Institute and the University of Helsinki are members of the EC-Earth consortium. To ensure comparable statistical properties from the CMIP6 database, the model-derived time series spans from January 1979 to December 2014. Modeled time series are linked to a real calendar, but they may not accurately reflect inter-annual variability in the real world. The spatial coverage is 40° N–90° N, including all the areas in the Arctic Ocean where sea ice might occur. For all the sea ice data in selected CMIP6 models, we used the first three available ensemble members (realizations) for each model, to help assess the impact of internal variability on long term trends.

For sea ice extent, we use the variables 'siconc' (the percentage of grid cells covered by sea ice), and 'areacello' (grid cell area for ocean variables). The temporal resolution is monthly, and the CMIP model experiment name is 'historical.' For sea-ice thickness, we use the variable 'sivol' (sea ice volume per area). Similar to sea ice extent, the time resolution is monthly. For sea-ice motion, we use the variables 'siu' (East-West–Component of sea-ice velocity) and 'siv' (North-South–Component of sea-ice velocity). Here the

https://doi.org/10.1017/aog.2024.25 Published online by Cambridge University Press

temporal resolution is daily because the IABP data is available daily and because we need to capture observed and modeled sea ice motion at the same temporal scale.

Table 1 shows some key properties of the models (Wu and others, 2018; Dix and others, 2019; Jungclaus and others, 2019; Parodi-Perdomo, 2019; Seland and others, 2019). Most of the selected CMIP6 models use Elastic-Viscous-Plastic rheology (EVP), except the MPI-ESM1-2-HR model which uses visco-plastic rheology.

Analysis method

We calculate sea ice extent based on sea-ice concentration data and grid cell area for both observational data and CMIP6 model data. We generate a dynamic mask based on the definition provided by Kern and others (2019), They demonstrated that the SIE should be computed as the total area of all grid cells where the sea-ice area fraction exceeds 15%. SIE is calculated in the range of 40° N to 90° N.

To examine regional differences in the models' skill in simulating sea ice characteristics, we divide the Arctic Ocean into three regions according to Maeda and others (2020). Region 1 (70° N to 80° N, 120° W to 180° W) includes the Chukchi Sea and the Beaufort Sea. Region 2 (70° N to 80° N, 100° E to 180° E) includes the Laptev Sea and East Siberian Sea, which are dominated by first and second-year ice. Region 3 (80° N to 90° N) is the central Arctic (Fig. 1).

For sea ice thickness and sea ice motion, we first convert the data into monthly averages and then calculate the regional mean in regions 1, 2, and 3 to generate time series. We calculate the monthly regional mean sea ice thickness (SIT_{mean}) as the ratio of the total sea ice volume (SIV_{total}) to the total sea ice area (SIA_{total}) in region 1, region 2 and region 3 respectively, over 36 years:

$$SIT_{\mathrm{mean}}(yr, mn) = \frac{SIV_{\mathrm{total}}(yr, mn)}{SIA_{\mathrm{total}}(yr, mn)}.$$

Here yr represents the year index (ranging from 1 to 36) and mn represents the month index (ranging from 1 to 12). We calculate the monthly regional mean sea ice motion (sea ice drifting speed) by averaging over all the data points that fall in region 1, region 2 and region 3 respectively.

We perform linear regression between ice parameters and time, calculating trends in the summer months (from June to September) and in the winter months (from January to April).

IABP buoy data points are distributed unevenly. In different years, the number of buoys and the routes of buoy deployment vary. We generate a $1^\circ \times 1^\circ$ latitude–longitude grid, sum the values in each grid cell, and calculate the mean value of drift speed where there are at least two data points in the grid cell. It is important to note that values above 0.5 m/s are not taken into account due to possible anomalous values caused by buoy position errors or by drifting in open water.

Figure 1. Arctic Sea segregation. Green patch represents region 1 (70° N to 80° N, 120° W to 180° W), orange patch represents region 2 (70° N to 80° N, 100° E to 180° E) and blue patch represent region 3 (80° N to 90° N).

In ACCESS-CM2, NorESM2-LM, and EC-Earth3 models, sea-ice drift speed is provided as a scalar quantity that can be used directly, while in the BCC-CSM2-MR, MPI-ESM1-2-HR, and IABP buoy data, sea-ice velocity data are provided in daily means. These are used in the calculation of drift speed.

We generate relative differences for sea ice extent, thickness and motion to validate each of the selected CMIP6 models: First calculating the mean value of sea ice parameters in each month from 1979 to 2014; Then we calculate the deviation from the mean value. In addition, we calculate the propagation of uncertainty (Kirchner, 2001) for the deviation rate of sea ice variables due to the uncertainties in both reference and model data.

Since model time series are only 36 years long, differences between members of the ensembles and models are assumed to describe merely the internal variability of the models rather than any natural variability. Therefore, we use standard deviation of the ensembles ($\pm 2\sigma_{ensemble}$) as a criteria to assess the plausibility of the models. We derived $\sigma_{ensemble}$ by first calculating the mean value from 36 years for each ensemble member in each month, and then calculating the standard deviation between the three ensemble members using Bessel's correction as in (Notz and SIMIP community, 2020).

We perform Theil-Sen regression (Theil, 1992) when calculating the trend of sea ice speed between 1979 and 2010. We conduct OLS regression (Zdaniuk, 2014) between SIT and sea ice drifting speed separately for the warm and cold seasons. We check the

Table 1. Properties of the five selected CMIP6 models EC-Earth3, ACCESS-CM2, BCC-CSM2-MR, MPI-ESM1-2-HR and NorESM2-LM, including model spatial resolution and sea ice physics

Model name	Spatial resolution (km)	Sea ice physics
EC − Earth3	100	The conservation of horizontal momentum, EVP rheology, and energy-conserving halo-thermodynamics (Vancoppenolle and others, 2009; Doscher and others, 2022)
ACCESS − CM2	250	EVP rheology, multi-layer thermodynamics (Bi and others, 2020)
BCC − CSM2 − MR	100	EVP rheology, Semtner's thermodynamic process (Semtner, 1976; Wu and others, 2018)
MPI − ESM1 − 2 − HR	50	Visco-plastic rheology (Hibler, 1979), zero-layer, mono-category thermodynamic model (Semtner, 1976; Mauritsen and others, 2019)
NorESM2 − LM	100	EVP rheology, mushy-layer thermodynamics (Hunke and Lipscomb, 2010; Seland and others, 2020)

https://doi.org/10.1017/aog.2024.25 Published online by Cambridge University Press

correlation between SIT and sea ice motion using reference data (PIOMAS-IABP/PIOMAS-PIOMAS), then check the correlation between modeled SIT and sea ice motion, and compare the results. In our analysis, sea ice motion acts as a dependent variable whilst SIT act as the independent variable. We choose to use Theil-Sen regression in this study as it is a method suitable for choosing the median slope when fitting a line, and because it has the advantage of minimizing the effect of outliers. The independent samples t-test is used as a statistical method for statistical checking the significance of regression results is the independent samples t-test.

Results

Sea ice extent

In general, each of the selected CMIP6 models reproduces the observed seasonal variation in Arctic sea ice extent (Fig. 2). There exists notable discrepancies within some months with the observations. In order to quantify the skill of each model in reproducing the seasonal evolution of sea ice extent, we calculate these biases for each of the models (Table 4). We consider model outputs to be plausible if they are within two standard deviations of the observed mean SIE.

The selected models exhibit different biases, as shown in Fig. 3. EC-Earth3 shows a one-month shift of minimum sea ice extent. This is possibly due to the cold bias of EC-Earth that can cause the ocean surface layer to freeze too early (Palmeiro and others, 2023). In Fig. 4, wherever the model ensemble mean falls within $\pm 2\sigma$ of the plausible range we infer that the model provides a plausible estimate. Thus EC-Earth3 provides plausible estimates in all 12 months, ACCESS-CM2 overestimates SIE from January to July, BCC-CSM2-MR model constantly underestimates through out the year, and the MPI-ESM1-2-HR model underestimates SIE from July to April. NorESM2-LM underestimates from December to July, but overestimates ice extent in September and October. Thus NorESM2-LM underestimates the amplitude of the seasonal cycle in SIE. Common to all models is that the largest deviations from observed SIE occur in September, which is the month of minimum ice extent.

In Fig. 5 we examine the trend in SIE. In the observations, sea ice extent has a decreasing trend of -0.59×10^6 km^2/decade. In the EC-Earth3 model, the decreasing trend varies among ensemble members, but all ensemble members fall in the plausible range of the trend. All the other models show a slower decrease than observations. For each of ACCESS-CM2, BCC-CSM2-MR and MPI-ESM1-2-HR, only one ensemble member falls outside the

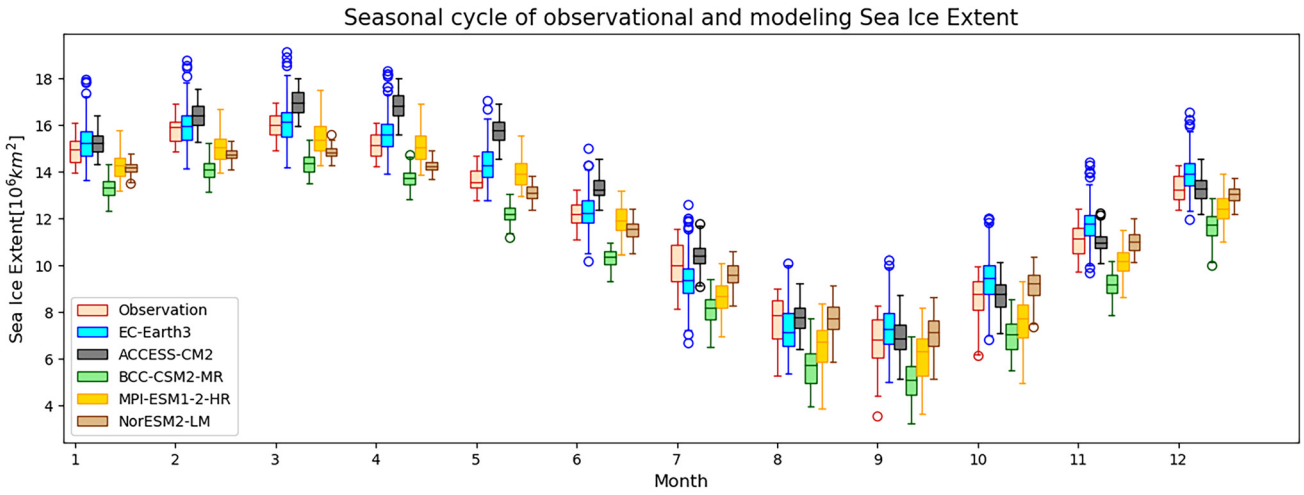

Figure 2. Seasonal cycle of sea ice extent (SIE) over a 36-year period from 1979 to 2014. The red box represents the observational SIE, including SIE data derived from satellite in 36 years. Boxes in other colors represent the SIE derived from the five selected models EC-Earth3, ACCESS-CM2, BCC-CSM2-MR, MPI-ESM1-2-HR, and NorESM2-LM, each incorporating data from 36 years across three model ensemble members.

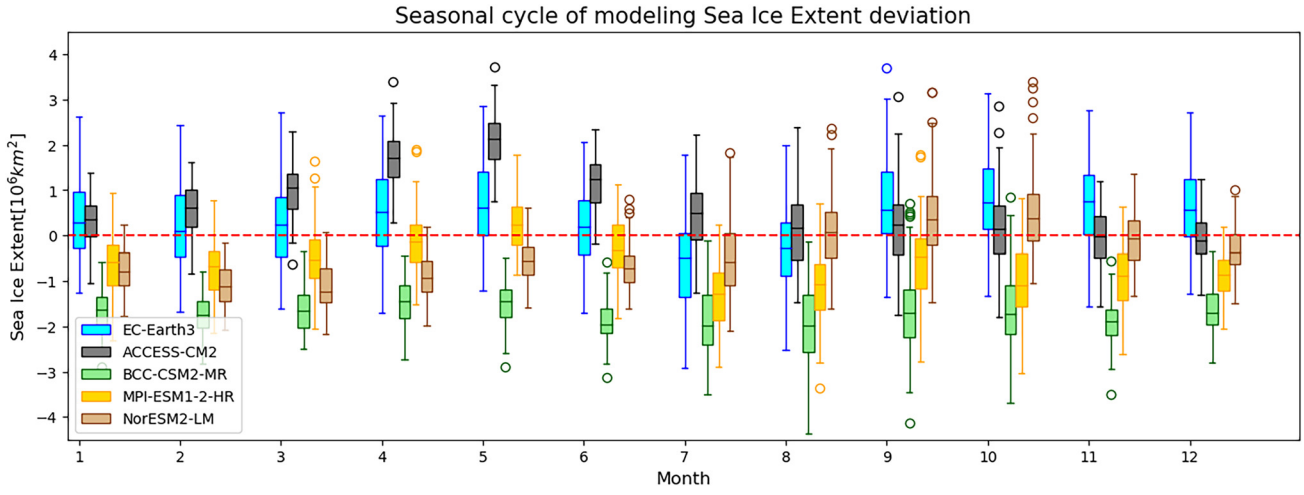

Figure 3. Seasonal cycle of the difference between modeling sea ice extent(SIE) and observational SIE over a 36-year period from 1979 to 2014. The boxes in different colors represent modeled SIE minus observed SIE derived from the five selected models EC-Earth3, ACCESS-CM2, BCC-CSM2-MR, MPI-ESM1-2-HR, and NorESM2-LM, each incorporating data from 36 years across three model ensemble members.

https://doi.org/10.1017/aog.2024.25 Published online by Cambridge University Press

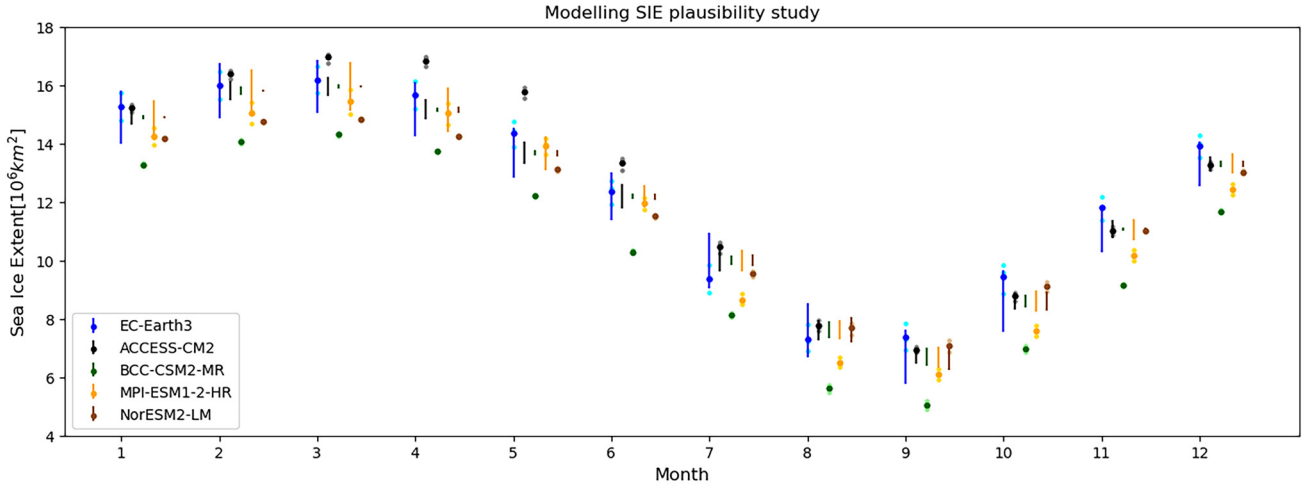

Figure 4. Examination of modeling SIE plausibility. The bars are centered around the observation mean SIE. The bars in different colors denote the ±2σ plausible range reflecting internal variability of three ensembles in five selected models EC-Earth3, ACCESS-CM2, BCC-CSM2-MR, MPI-ESM1-2-HR, and NorESM2-LM. The dots with the same color as the bars represent the model ensemble mean, and the dots with lighter colors represent three different ensemble members.

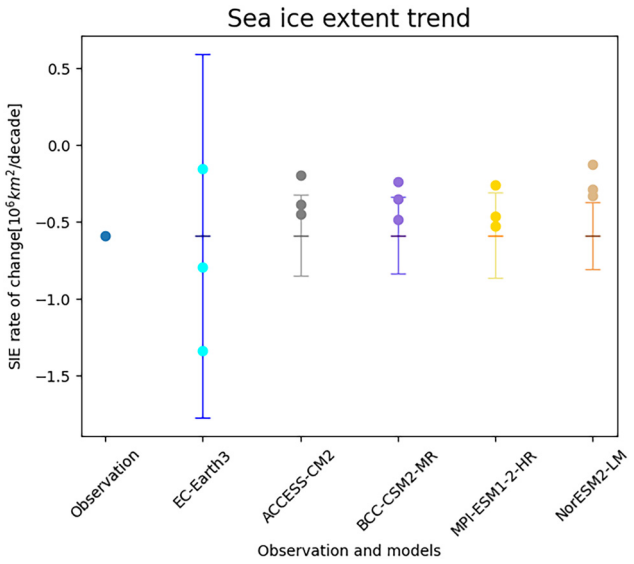

Figure 5. Trends of sea ice extent (SIE) over the period from 1979 to 2014. The observational SIE trend is depicted as a distinct dot on the left side of the figure. On the left of the figure is dots representing trend calculated from model simulation. The five different colors represent five CMIP6 models: EC-Earth3, ACCESS-CM2, BCC-CSM2-MR, MPI-ESM1-2-HR, and NorESM2-LM, Each model encompasses three ensemble members. The error bars are the plausible range of modeled trend, which is double the standard deviation of three model ensembles.

plausible range. However in NorESM2-LM, all of the ensemble member trends fall outside the plausible range.

In our selected CMIP6 models, other than EC-Earth3, the rate of decrease does not vary substantially among ensemble members. However we note that three members is a small number with which to examine the internal variability of a model, and that the failure to 'bracket' observed trends may be due in large part to this small number of members. In the MPI-ESM1-2-HR, ACCESS-CM2, BCC-CSM2-MR and EC-Earth3 models, all three ensemble members have higher inter-annual variability than the satellite observations, while all three ensemble members in NorESM2-LM have smaller inter-annual variability than observations.

Sea ice thickness

We compare CMIP6-simulated SIT with PIOMAS data and calculate deviation rates in three defined regions.

Figure 6 shows the seasonal cycle of sea ice thickness in PIOMAS and in selected CMIP6 model outputs for (a) region 1, (b) region 2, and (c) region 3. Figure 7 shows the difference in SIT between selected models and PIOMAS. Figure 8 shows the plausible estimation range (defining a model deviation from the PIOMAS average of below ±2σ as a plausible estimate) for each model in the three regions, and reveals whether the model simulation falls in this range. Table 5 details the deviations when comparing CMIP6 SIT with PIOMAS, and also provides the associated uncertainties.

We conclude from Fig. 8 and Table 5a that: In region1 (covering the Chukchi Sea and the Beaufort Sea), ACCESS-CM2 overestimates SIT all year round, EC-Earth3 overestimates SIT from May to November, and NorESM2-LM overestimates SIT from June to November. BCC-CSM2-MR and MPI-ESM1-2-HR underestimate SIT all year-round.

From Fig. 8 and Table 5b, we conclude that in region2 (covering the Laptev Sea and the East Siberian Sea), the EC-Earth3 and ACCESS-CM2 models both overestimate SIT throughout the year, while the NorESM2-LM model overestimates SIT in February and March, and from June to October. BCC-CSM2-LM underestimates SIT all year-round, while MPI-ESM1-2-HR model underestimates SIT from July to December.

From Fig. 8 and Table 5c, we conclude that in region3 (covering the central Arctic), EC-Earth3 and NorESM2-LM overestimate SIT from July to September and from June to October respectively. The BCC-CSM2-MR and MPI-ESM1-2-HR models underestimate SIT all year-round. Finally, ACCESS-CM2 provides plausible estimates throughout the entire year.

None of the models produce a perfect simulation result throughout the whole year and across the three regions, but the reference data lie within the range of selected CMIP6 models. Among all the models, the BCC-CSM2-MR model produces the thinnest ice thickness output, while EC-Earth3 yields the thickest. The BCC-CSM2-MR and MPI-ESM1-2-HR models tend to underestimate thickness, while EC-Earth3, ACCESS-CM2, and NorESM2-LM models tend to overestimate thickness. The models show a tendency to exhibit higher deviations during the warm season when ice is thin, and to perform better in simulating the thicker ice prevailing during the cold season. Uncertainties in model-observation deviations remain extremely high throughout the year, but especially in the summer months. In part this results from the inherent measurement uncertainties in the original SIT datasets. However there is an additional source of uncertainty, as

https://doi.org/10.1017/aog.2024.25 Published online by Cambridge University Press

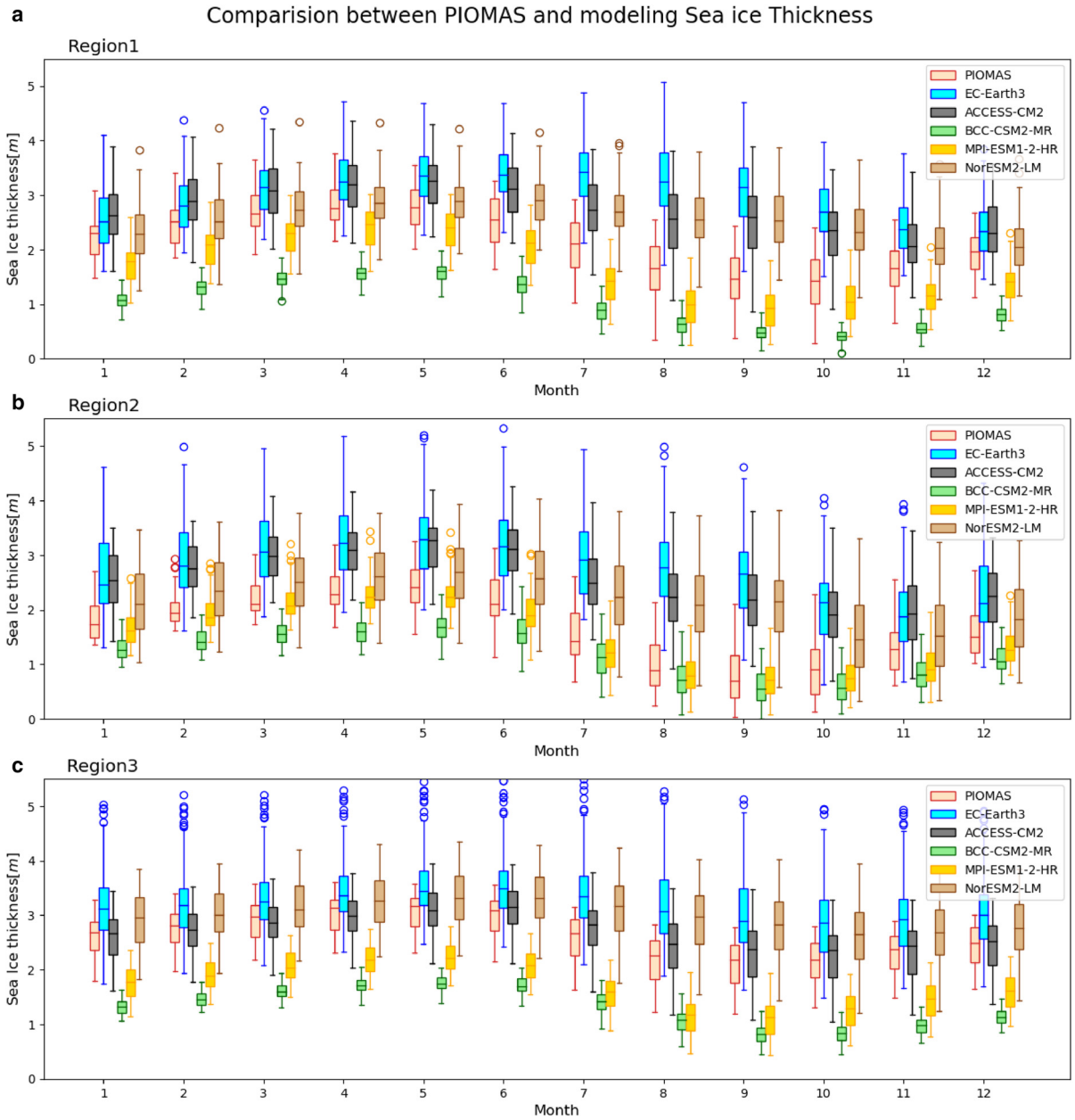

Figure 6. Seasonal cycle of PIOMAS and modeling sea ice thickness over a 36-year period from 1979 to 2014 in (a) region 1, (b) region 2, (c) region 3, shown in box plot format. The red box includes SIT derived from PIOMAS data in 36 years time span, boxes in other colors represent the SIT derived from the five selected models EC-Earth3, ACCESS-CM2, BCC-CSM2-MR, MPI-ESM1-2-HR, and NorESM2-LM, each incorporating data from 36 years across three model ensemble members.

we analyze monthly and regional averages, which do not fully capture the substantial spatial and temporal variations present both in models and observations.

Figure 9 compiles the trends in sea ice thickness (both PIOMAS and CMIP6 models) across (a) Region 1, (b) Region 2, and (c) Region 3. The summer and winter trends are shown separately in the plot. PIOMAS results show that sea ice exhibits a more rapid thinning trend in the summer than in winter, and most of the CMIP6 models capture this phenomenon. The magnitudes of the thinning trends calculated from PIOMAS also fall in the range of the CMIP6 model spread. The BCC-CSM2-MR and MPI-ESM1-2-HR models consistently underestimate the rate of thinning while EC-Earth3 tends to overestimate this trend. Regional differences are not substantial.

Figure 10 comprises a regional comparison between the selected CMIP6 model simulations and PIOMAS results. The latter indicate that sea ice is thickest in the central Arctic (region 3), followed by region 1, with the thinnest sea ice occurring in region 2. Sea ice is thinner during summer months, and the regional difference is more considerable. Sea ice is thicker during winter months, and the regional difference is smaller. While both EC-Earth3 and Nor-ESM2-LM capture the regional distribution of SIT seen in the reference data, they still underestimate the extraordinarily thick ice in the central Arctic (region 3). The remaining CMIP6 models are unable to simulate regional variations similar to those in PIOMAS. Furthermore, none of the models effectively reproduces the larger summertime regional variation in SIT. The majority of the selected CMIP6 models show only a small decreasing trend in SIT.

Sea ice motion

In this section, we investigate the performance of CMIP6 models when simulating Arctic sea ice motion by comparing their outputs with data from IABP buoys. We focus on three different Arctic regions and analyze the results from five CMIP6 models: EC-Earth3, ACCESS-CM2,

https://doi.org/10.1017/aog.2024.25 Published online by Cambridge University Press

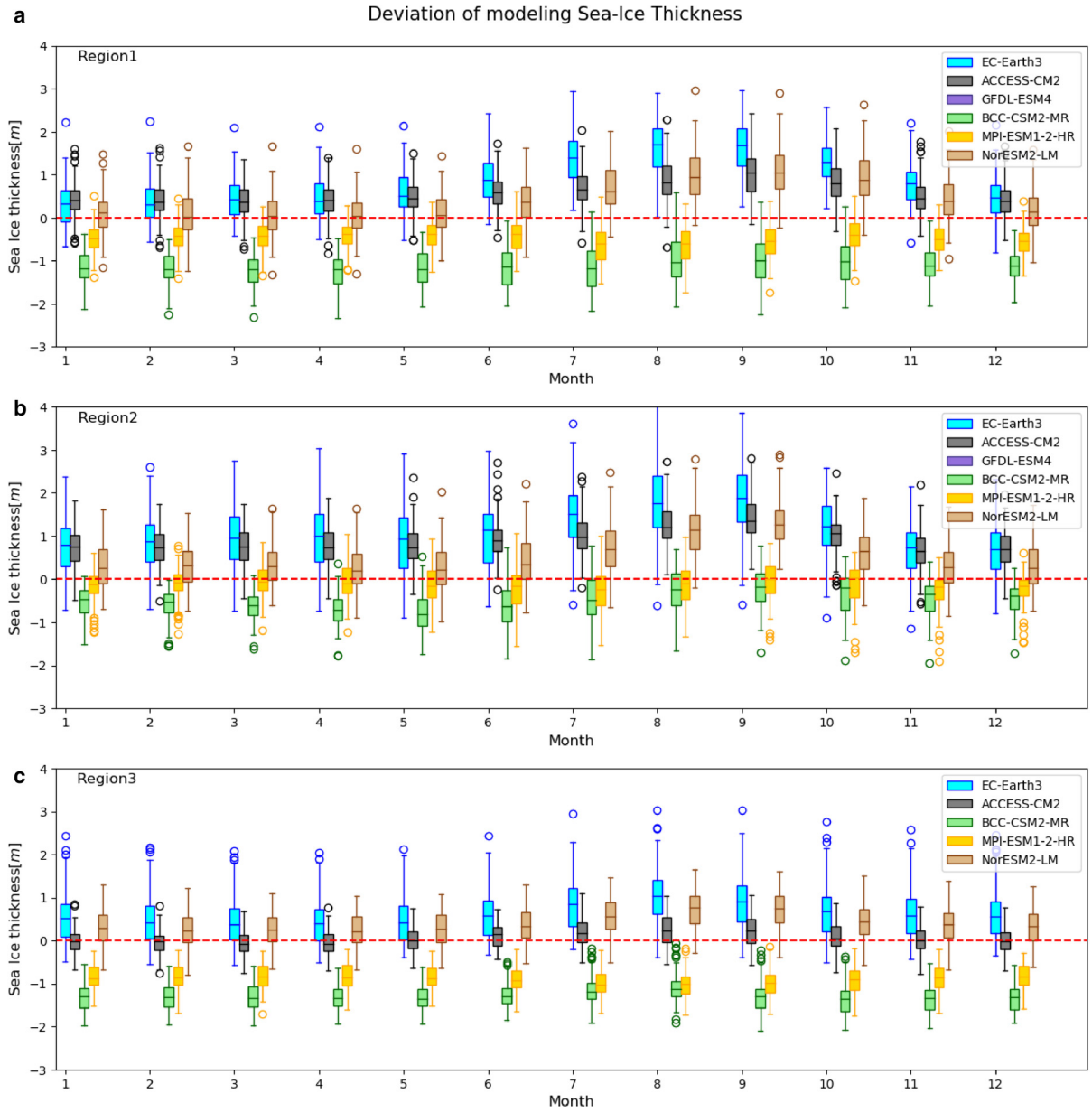

Figure 7. Seasonal cycle of difference between modeling sea ice thickness an PIOMAS(model minus PIOMAS) over a 36-year period from 1979 to 2014 in (a) region 1, (b) region 2, (c) region 3, shown in box plot format. Boxes in five colors represent the deviation of sea ice thickness in the five selected models EC-Earth3, ACCESS-CM2, BCC-CSM2-MR, MPI-ESM1-2-HR, and NorESM2-LM, each incorporating data from 36 years across three model ensemble members.

BCC-CSM2-MR, MPI-ESM1-2-HR, and NorESM2-LM. Our analysis of sea ice motion is restricted to sea ice speed.

To validate the models, we compare their seasonal cycles and sea ice drift speed against buoy data. In addition, we examine the regional distribution of sea ice drift speed and the trend of sea ice motion in different regions, again comparing the selected CMIP6 model simulations against IABP output.

We focus in particular on the months of April and October, which comprise the melting season and freezing seasons respectively. First, we compare the sea ice speeds between the models and the buoy data. We calculate the correlation coefficient between SIE and SIT for each of the selected CMIP6 models, for satellite data, and for PIOMAS. The resulting value is 0.85, and this indicates a high dependency between SIE and SIT. Given this correlation, and in the absence of a hypothesis that supposes ice extent to affect ice motion, we study only the correlation between sea ice motion and SIT. Finally we study the correlation between SIT and SISPEED within selected CMIP6 models and also using the reference data(PIOMAS-IABP/PIOMAS-PIOMAS).

Table 2 shows the months when sea ice speed reaches its maximum and its minimum speeds within each model and in the reference data. Figure 11 shows the the seasonal cycle of sea ice speed in IABP and selected CMIP6 model outputs in (a) region 1, (b) region 2, and (c) region 3. Figure 12 shows the anomaly in sea ice speed between the selected models and IABP. The minimum sea ice motion occurs in March (region 1, region 2) or April (region 3), while the maximum sea ice motion occurs in August (region 2) and September (region 1, region 3). In general, the modeled seasonal cycles of sea ice motion are shifted later than the IABP observations but remain within an acceptable range, typically lagging by 1-2 months. However, the MPI-ESM1-2-HR model is an exception, as it clearly deviates from the observed data, indicating a substantial failure in accurately capturing the seasonal cycle (Fig. 11, Table 2). Figure 13 examines the plausible estimation range for sea ice speed within each model for the three regions, and reveals whether the model simulation falls in this range. Meanwhile Table 6 includes the deviations when comparing CMIP6 sea ice speed

https://doi.org/10.1017/aog.2024.25 Published online by Cambridge University Press

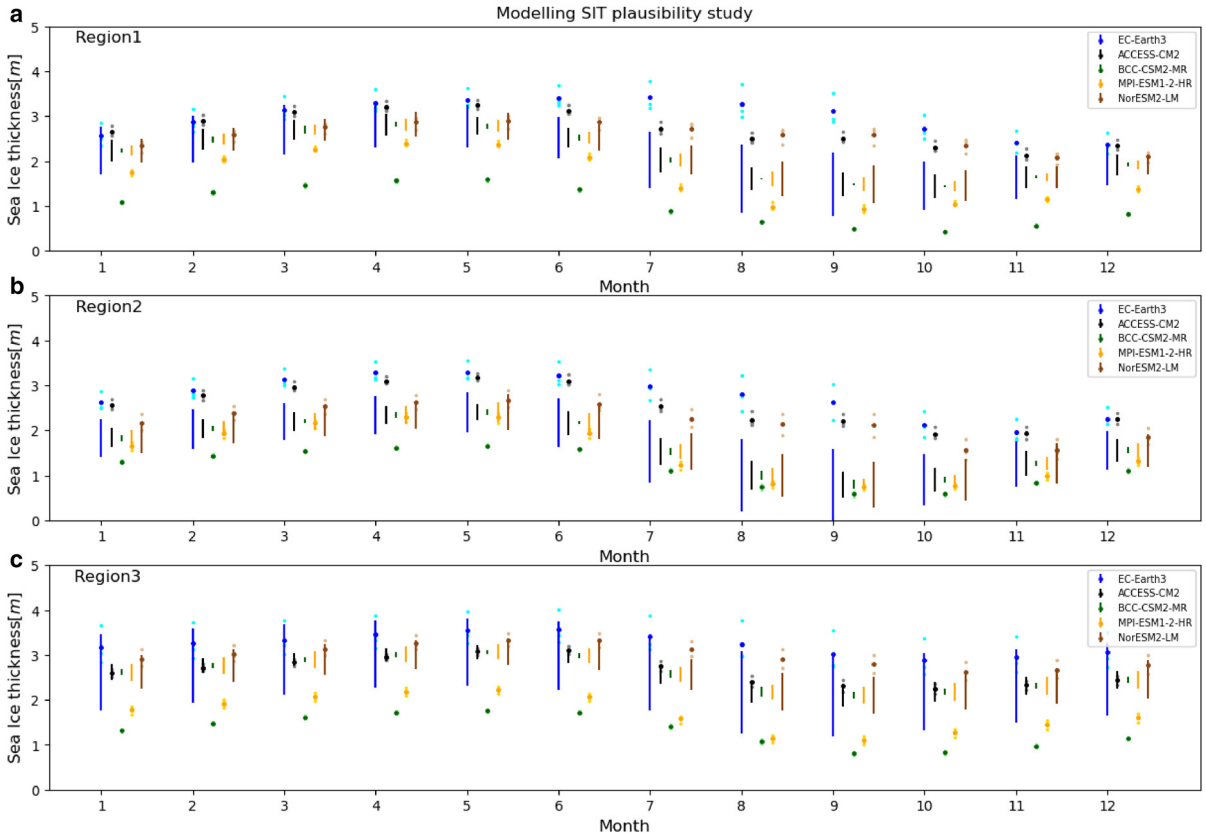

Figure 8. Examination of modeling SIT plausibility in (a) region 1, (b) region 2, (c) region 3. The center of all the bars are PIOMAS average.The bars in different colors denote the $\pm 2\sigma$ plausible range reflecting model internal variability of three ensembles in five selected models EC-Earth3, ACCESS-CM2, BCC-CSM2-MR, MPI-ESM1-2-HR, and NorESM2-LM. The dots with the same color as the bars represent the model ensemble mean, and the dots with lighter colors represent different ensembles.

with IABP, as well as the associated uncertainties. Notably, MPI-ESM-1-2-HR exhibits the highest deviation across the entire Arctic region due to its failure in simulating the seasonal cycle of sea ice motion.

From Fig. 13 and Table 6, we conclude that in coastal seas (region1, region2), the selected CMIP6 models tend to overestimate SIM in the first half of the year and underestimate it in the second half of the year. This is due to the small seasonal

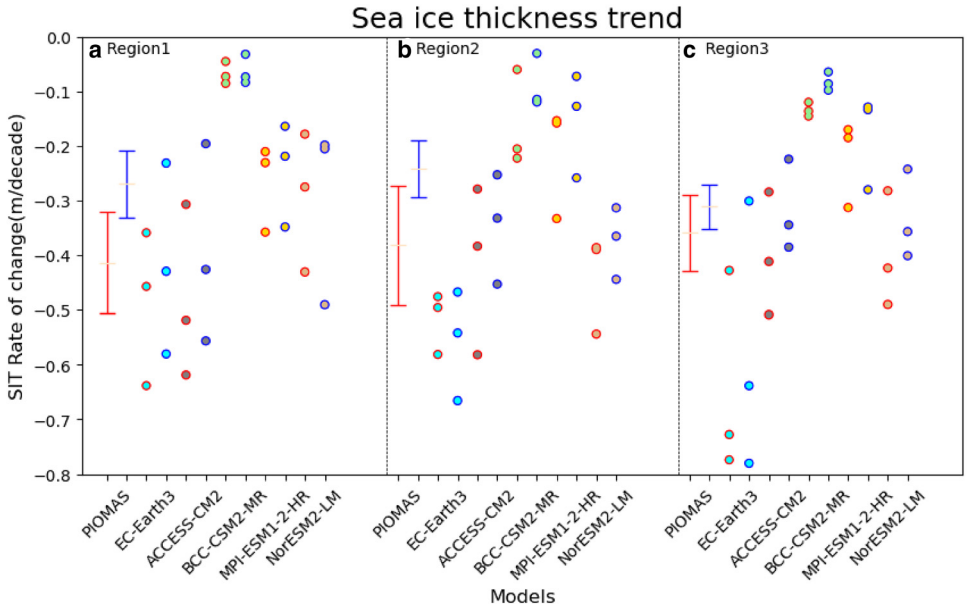

Figure 9. Trends of sea ice thickness in PIOMAS and 5 CMIP6 models (three ensemble for each model) between 1979 and 2014 with units of m/decade in (a) region 1, (b) region 2, and (c) region 3 in both summer and winter. PIOMAS SIT trends are represented by error bars, red bars mean the range of summer SIT trend, blue bars mean the plausible range of winter SIT trend. Model trends are represented by scatter plots. The red edge color represents modeled SIT trend in summer months, the blue edge color represents modeled SIT trend in winter months, and the different face-colors of the boxes represent different CMIP6 models, denoted by *x*-axis.

https://doi.org/10.1017/aog.2024.25 Published online by Cambridge University Press

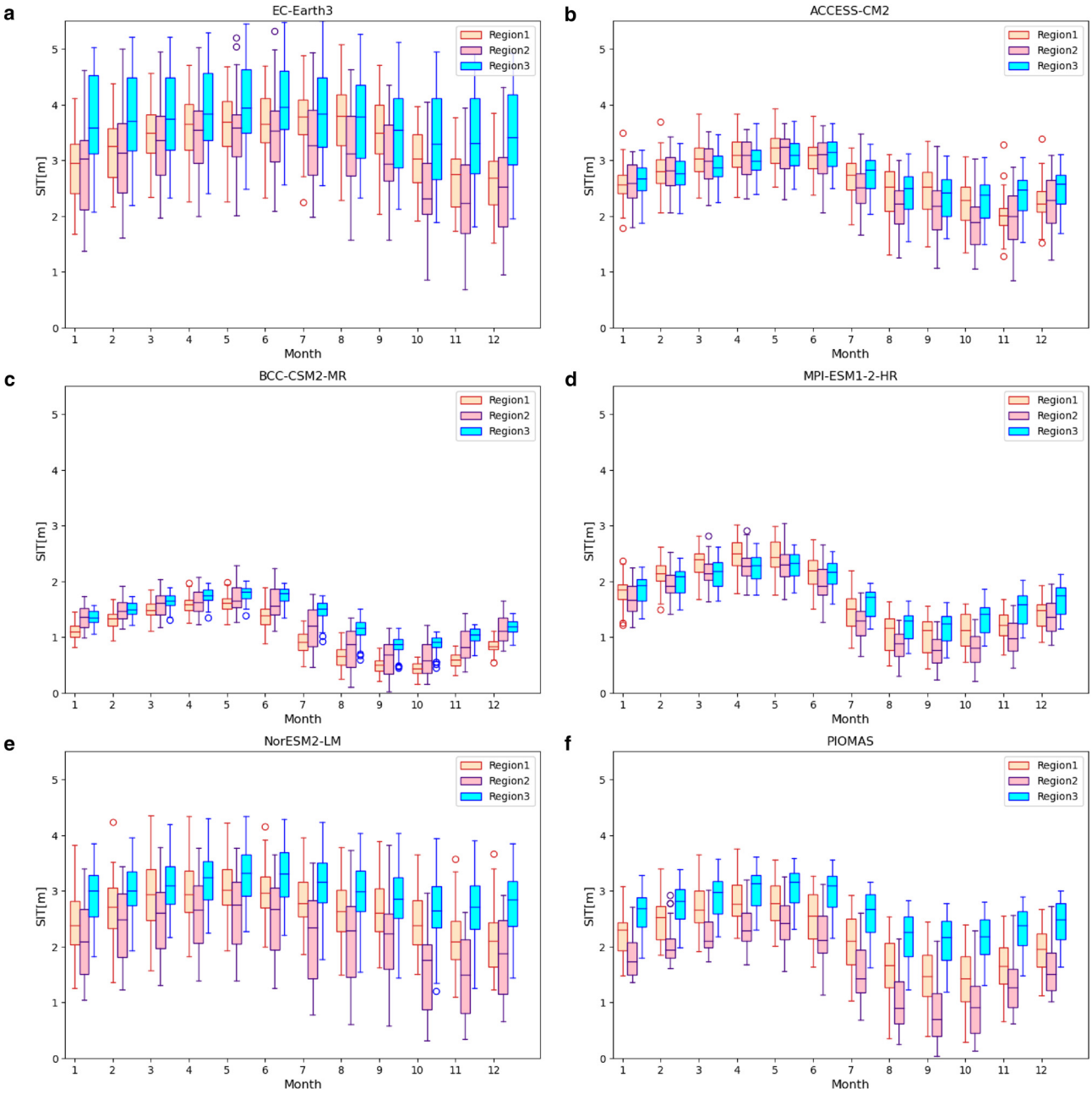

Figure 10. Regional comparison of monthly averaged SIT among region 1, region 2 and region 3 in the whole year, incorporating both five CMIP6 models (a) EC-Earth3, (b) BCC-CSM2-MR, (c) ACCESS-CM2, (d) MPI-ESM1-2-HR, and (e) NorESM2-LM and (f) PIOMAS data. Red boxes represent region 1, pink boxes represent region 2 and blue boxes represent region 3.

cycle amplitude exhibited in the selected CMIP6 models. In the central Arctic (region3), all the selected CMIP6 models have the tendency to overestimate SIM. The NorESM2-LM model provides the most accurate simulation among the selected models, assessed by the number of plausible estimations.

To analyze the sea ice evolution in the Arctic, we again focus on April and October. This is in part because they are close to the minimum and maximum, respectively, of sea ice motion, and in part to maintain consistency with the analysis of SIT and SIE. Figure 14 shows the distribution of the trend and its significance

Table 2. Maximum and minimum sea ice drifting speed in the seasonal cycle in IABP, EC-Earth3, ACCESS-CM2, BCC-CSM2-MR, MPI-ESM1-2-HR and NorESM2-LM models in region 1, region2 and region3

Region 1			Region 2			Region 3		
Data	Min	Max	Data	Min	Max	Data	Min	Max
IABP	3	9	IABP	3	8	IABP	4	9
EC-Earth3	4	11	EC-Earth3	4	9	EC-Earth3	5	8
ACCESS-CM2	3	9	ACCESS-CM2	3	8/9	ACCESS-CM2	5	9
BCC-CSM2-MR	5	10	BCC-CSM2-MR	5	10	BCC-CSM2-MR	5	10
MPI-ESM1-2-HR	6	11	MPI-ESM1-2-HR	6	11	MPI-ESM1-2-HR	7	11
NorESM2-LM	3	10	NorESM2-LM	2	10	NorESM2-LM	5	10

https://doi.org/10.1017/aog.2024.25 Published online by Cambridge University Press

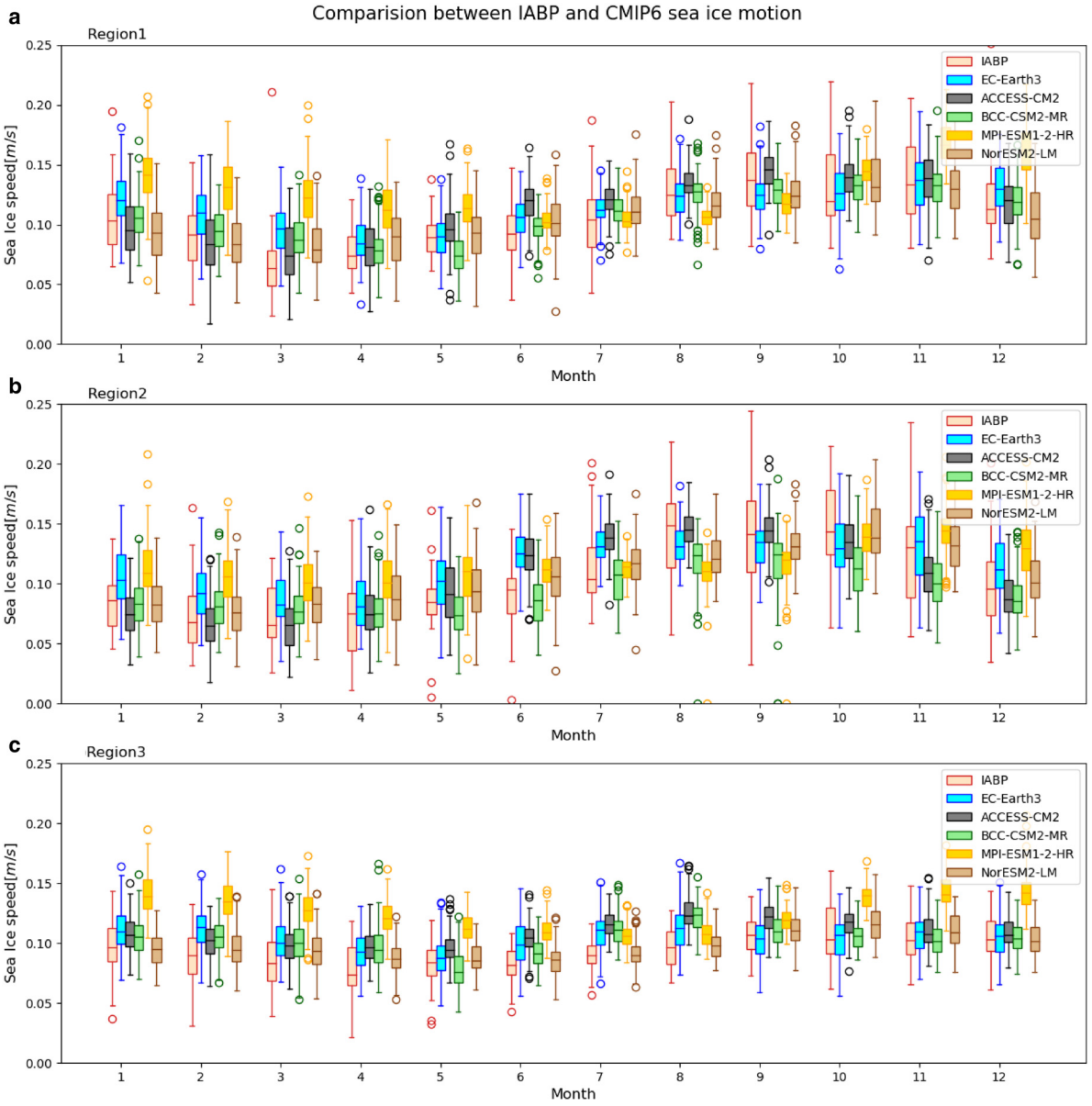

Figure 11. Seasonal cycle of IABP and modeling sea ice motion from five selected CMIP6 models over a 36-year period from 1979 to 2014 in (a) region 1, (b) region 2, (c) region 3, shown in box plot format. The red box represents sea ice drifting speed derived from IABP data incorporating data in 36 years, boxes in other colors represent the sea ice speed derived from the five selected models EC-Earth3, ACCESS-CM2, BCC-CSM2-MR, MPI-ESM1-2-HR, and NorESM2-LM, each incorporating data in 36 years across three model ensemble members.

in sea ice drifting speed from 1979–2021 in IABP data in both April and October. We use areas where sea ice concentration is 85% to represent the ice edge. This is done in order to eliminate data points in open water and thus reduce uncertainties arising from buoys unrepresentative of ice motion. The significance of the trend is shown in *p*-value format in the lower part of Fig. 14 – when *p*-value is less than 0.05, the trend is significant. A widely distributed increasing trend is observed in both months; however, in April, the negative trend still exists near the Canadian Archipelago, in the East Siberian Sea and in the Greenland Sea. In October, the increasing trend of sea ice drifting speed is dominant in the marginal ice zone. In both months, the central Arctic region has the most complex distribution of trends in sea ice dynamics due to noise in the high Arctic. Buoy deployments are more sparse here, and, in addition, the grid cells cover less area at higher latitudes. Due to a combination of these two factors, the number density of observations over the 36 years decreases with increasing latitude, and with lower number density there are larger uncertainties in the high Arctic trend. The significant positive trend is focused in the Beaufort and Chukchi Seas (region1).

Rampal and others (2009) conducted research on the trend of average sea ice speed based on IABP buoy data. Winter sea ice exhibits a mean speed increase of 17% per decade (7.41×10^{-3} m/s per decade), and a summertime speed increase of 8.5% per decade (5.89×10^{-3} m/s per decade) during 1979–2007. We conduct an extension of the IABP data analysis to cover the years 1979–2021. Unlike (Rampal and others, 2009) who calculated the pan-Arctic mean trend, we have calculated trends for aforementioned three specific regions separately in the summer months (June–September) and winter months (January–April). Figure 15 shows the variation and trend of sea ice motion between 1979–2021 in summer and winter months averaged in region 1, region 2 and region 3.

In order to avoid noise disturbance, we also calculate low slope – the lower bound of the 95% confidence interval on slope – and high slope – the upper bound of the 95% confidence

https://doi.org/10.1017/aog.2024.25 Published online by Cambridge University Press

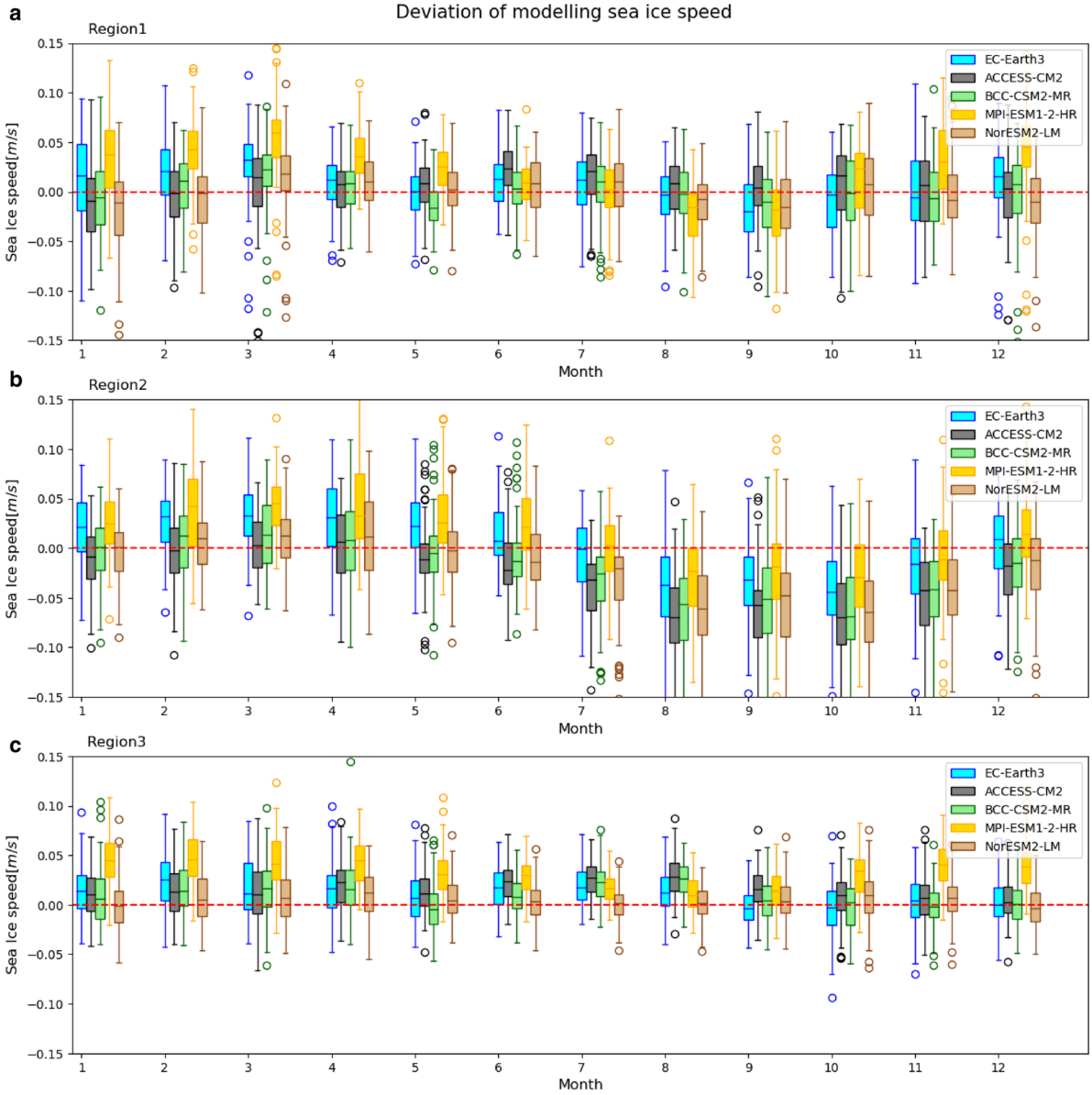

Figure 12. Seasonal cycle of difference between modeling sea ice speed and IABP (model minus IABP) over a 36-year period from 1979 to 2014 in (a) region 1, (b) region 2, (c) region 3, shown in box plot format. Boxes in five colors represent deviation of sea ice speed in five selected models EC-Earth3, ACCESS-CM2, BCC-CSM2-MR, MPI-ESM1-2-HR, and NorESM2-LM, each incorporating data from 36 years across three model ensemble members.

interval on slope – in region 1, region 2 and region 3; again treating the summer trend and winter trend separately. In region1 the summer trend's lower slope is 3.68×10^{-6} and the higher slope is 5.91×10^{-6}. The winter trend's lower slope is 2.13×10^{-6} and the higher slope is 3.93×10^{-6}. In region2 the summer trend's lower slope is 3.10×10^{-6} and the higher slope is 6.73×10^{-6}. The winter trend's lower slope is $2.25 \times 10^{-6}$and the higher slope is 4.81×10^{-6}. In region3 the summer trend's lower slope is 1.43×10^{-6} and the higher slope is 2.56×10^{-6}. The winter trend's lower slope is 1.35×10^{-6} and the higher slope is 2.99×10^{-6}.

In region 1, during the summer months, the sea-ice drifting speed increases at a rate of 0.014 m/s per decade, while in winter it increases at a rate of 0.010 m/s per decade. Meanwhile in Region 2, in summer, the sea-ice drifting speed increases at a rate of 0.018 m/s per decade and, during winter, increases at a rate of 0.009 m/s per decade. In region 3, the speed increases at a rate of 0.007 m/s per decade in summer, and increases at a rate of 0.006 m/s per decade. In coastal Arctic seas, mean sea ice speed is increasing much faster than in the central Arctic, especially in the Laptev and East Siberian seas. Furthermore, compared with (Rampal and others, 2009)'s result, sea ice motion is accelerating even more rapidly after 2007 – increasing at a rate of 0.024 m/s per decade in summer months and 0.022 m/s per decade in winter months (calculated from 2007–2021).

We examine CMIP6 model performance by comparing it against IABP data for sea ice motion in different regions (Fig. 16). Our analysis shows that the coastal Arctic seas exhibit large seasonal variations, particularly in region 2. In contrast, the central Arctic generally maintains a relatively steady state of sea ice motion throughout the year. Inside the marginal seas, region 2 displays higher motion during summer than region 1, while region 1 exhibits the faster ice motion in winter. During the seasonal transition phase, when sea ice motion shifts from a slow pattern to a fast pattern (e.g. April, May, and June), the regional difference is the smallest. Regarding the regional patterns in CMIP6 models, the models agree with reference data except for BCC-CSM2-MR and MPI-ESM1-2-HR, which fail to simulate the correct regional distribution of sea ice drifting speed.

Figure 17 presents the trends for sea ice motion in the IABP buoy data output, as well as for the first three ensemble members

https://doi.org/10.1017/aog.2024.25 Published online by Cambridge University Press

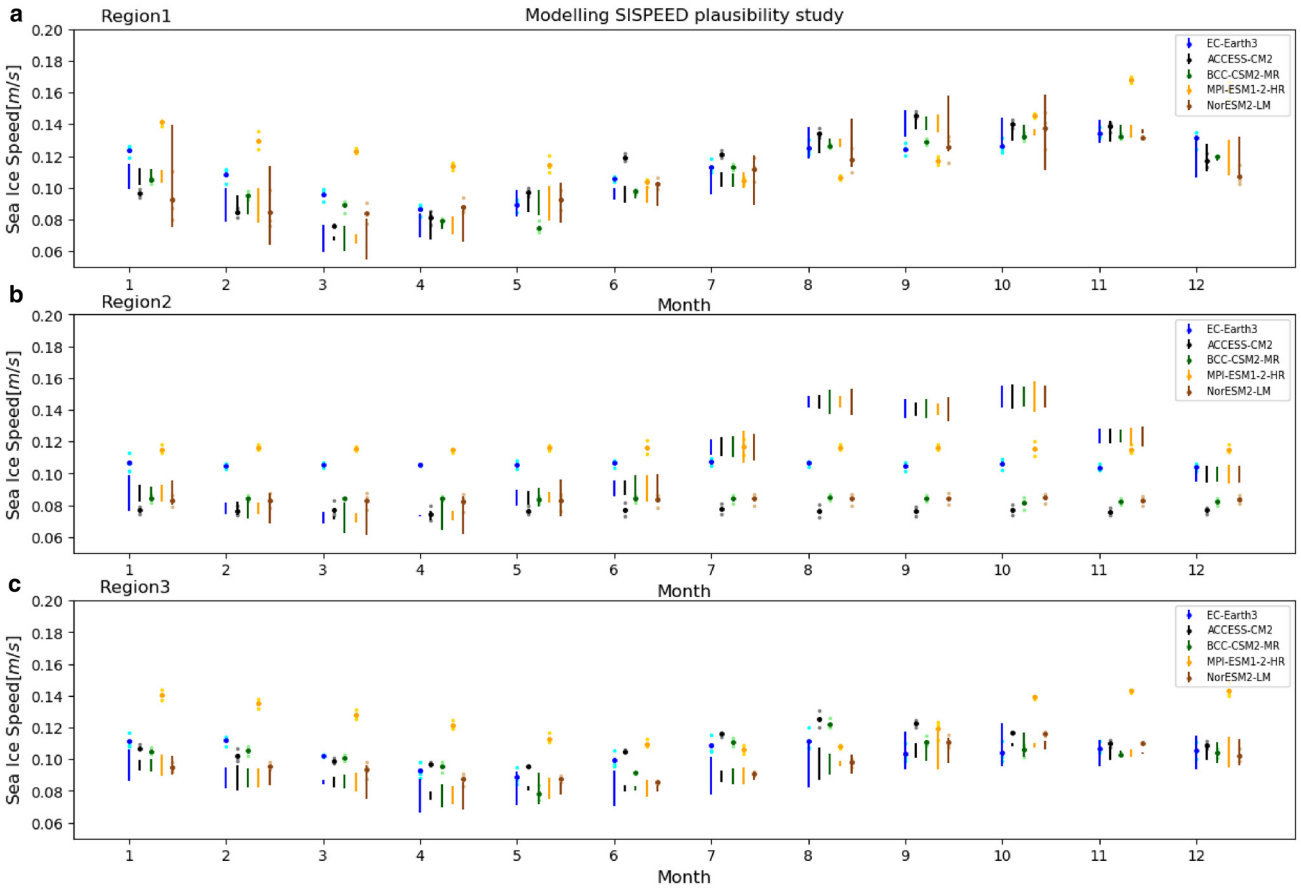

Figure 13. Examination of modeling sea ice speed plausibility in (a) region 1, (b) region 2, (c) region 3. The bars in different colors denote the ±2σ plausible range reflecting model three ensembles internal variability in five selected models EC-Earth3, ACCESS-CM2, BCC-CSM2-MR, MPI-ESM1-2-HR, and NorESM2-LM. The dots with the same color as the bars represent the model ensemble mean, and the dots with lighter colors represent different ensembles.

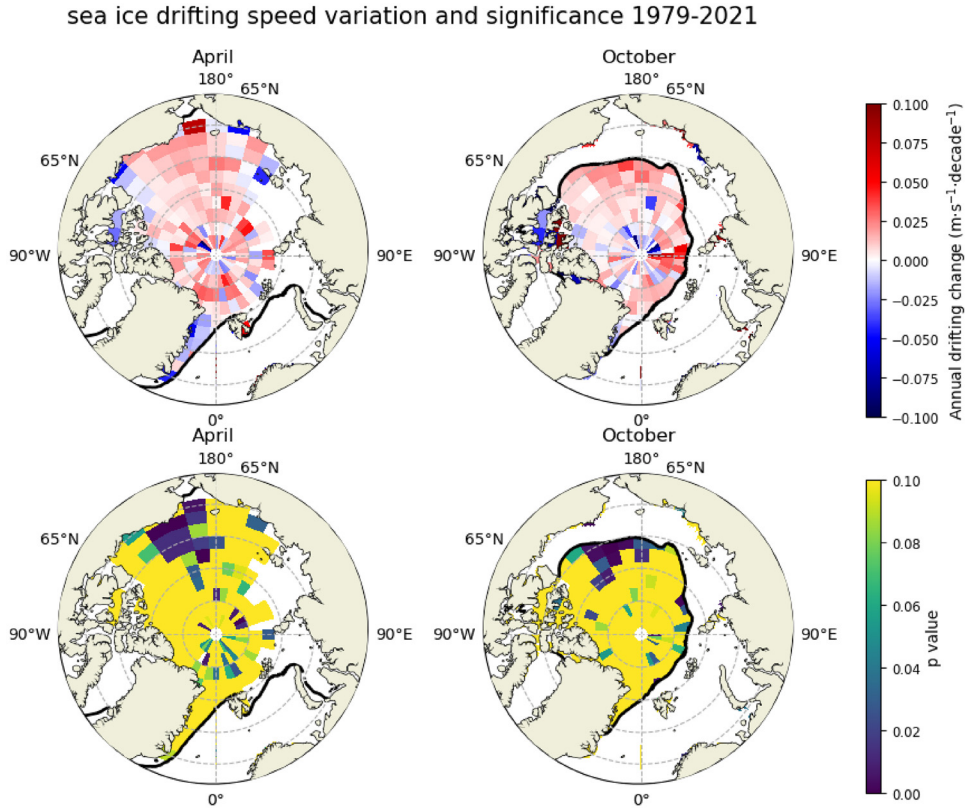

Figure 14. Distribution of annual sea ice drift speed rate of change (top) and its significance(bottom) over time period 1979–2021 in the Arctic Ocean in April (left panel) and October (right panel) calculated from IABP buoy data, the value indicate how much ice drifting speed change per decade on average, only grid cell which has more than 2 valid time stamp are taken into account, thick black line is the boundary where sea ice concentration is 85%, the reddish color indicates that sea ice drifting speed is increasing in those areas, while the bluish color indicates a decrease. Bottom plots are significance of trend shown as *p*-value. Sea ice drift speed is 0 at the pole because u,v is not defined there on a spherical grid. Noise around the pole is impacted by the regridding of the values.

https://doi.org/10.1017/aog.2024.25 Published online by Cambridge University Press

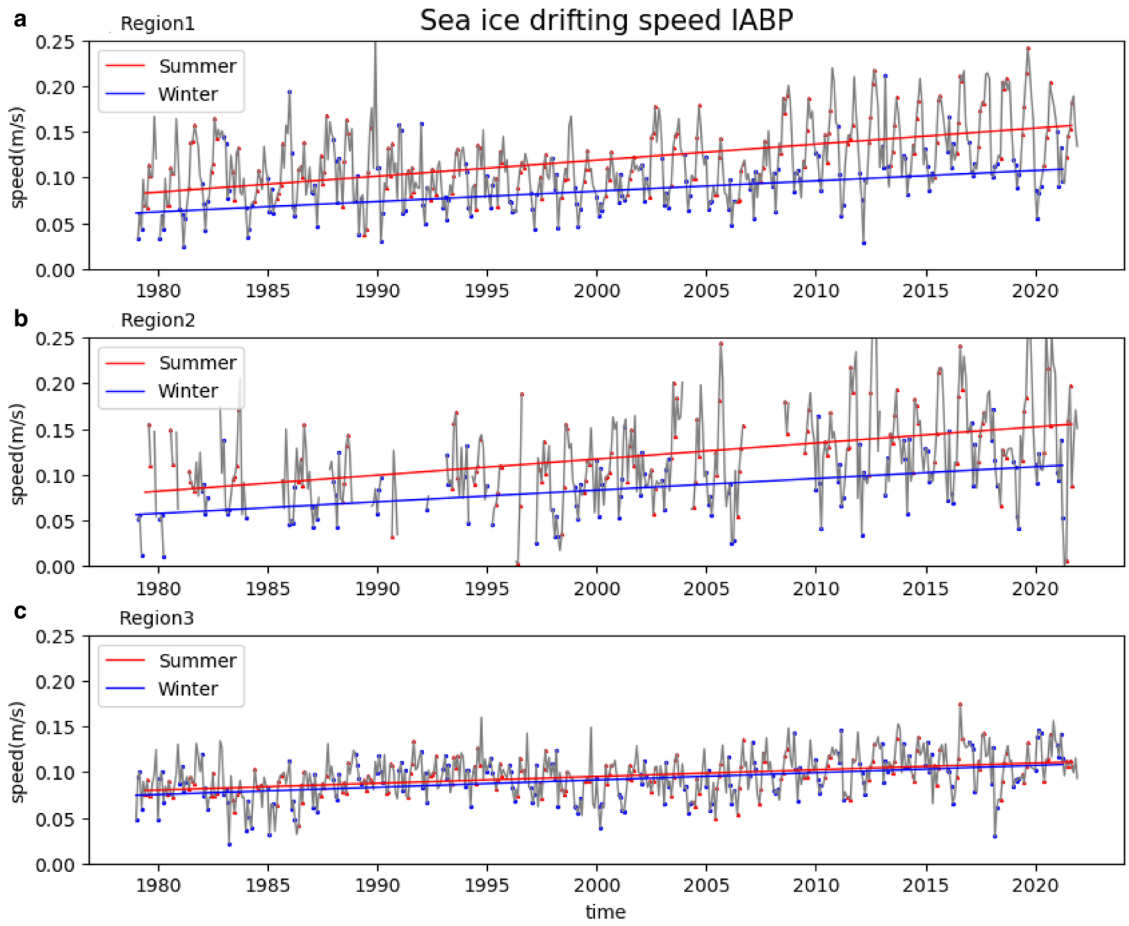

Figure 15. Annual variation and trend of IABP sea-ice drifting speed between 1979–2021 in (a) region 1, (b) region 2 and (c) region 3. The red line represents summer months (June-September) average, the blue line represents winter months (January–April) average, red dots are summer months, blue dots are winter months.

of the five selected CMIP6 models, from 1979 to 2014, focusing on (a) region 1, (b) region 2, and (c) region 3. The IABP results indicate that region 2 exhibits the fastest increase in sea ice motion, followed by region 1, and that region 3 has the slowest increase. Notably the IABP output reveals that summer months show a more rapid sea ice motion increase, especially in coastal Arctic seas, between 1979–2014. Most of selected CMIP6 models failed to simulate this feature.

Compared to the trend of sea ice motion in IABP buoy data, most model realizations underestimate the observed increase in ice motion. This is particularly evident in regions 1 and 2, which are predominantly covered by first and second year ice. In the Central Arctic region, only the EC-Earth3 captures an increasing trend of sea ice speed compatible with reference data (in that the ensemble mean trend in both summer and winter fall in the range of the IABP error bar).

These results indicate that CMIP6 models struggle to accurately reproduce regional variations in ice motion evolution, and that most of them severely underestimate the magnitude of trends in ice motion.

Again we focus on April and October when comparing the selected CMIP6 models with IABP. Figure 18 shows the model outputs and the IABP output in both April and October. In region 1, in both April and October, all models overestimate the median sea ice motion. In region 2, in October, CMIP6 models underestimate the median, whereas in April, they overestimate the median. Furthermore, the models exhibit much smaller seasonal variations than observations. In region 3, only EC-Earth3 and CSM2-MR models perform well in October; other models give overestimates. All models overestimate in April. The MPI-ESM1-2-HR model has the highest deviation from observations due to a severe misrepresentation of the seasonal cycle. Compared with observations, CMIP6 models have smaller seasonal cycle amplitudes. In general, models overestimate sea ice motion in April throughout the entire Arctic and, in region 2, underestimate sea ice motion in October.

Relations between sea ice properties

Kwok and others (2013) argued that changes in sea ice motion can be attributed to ice strength, which is dependent on sea ice thickness and concentration. Thus we conduct further examinations of the coupling between sea ice motion and sea ice state.

Sea ice thickness-motion coupling

Yu and others (2019) showed that there was a negative relationship between ice drift speed and thickness in summer months, as calculated by the coupled Arctic regional climate model HIRHAM-NAOSIM 2.0. We examine the relationship between SIT and SIM using PIOMAS and IABP data, which serve as reference data. We also use SIT and SIM data from five selected CMIP6 models to assess the correlation between modeled SIT and sea ice motion. We then compare the model-derived correlations with the reference data-derived correlations. The central Arctic region exhibit the least uncertainties in sea ice motion and thickness – due to its small number of open water grid points – so we only consider the ice covered grid points within the central Arctic region (80° N–90° N).

https://doi.org/10.1017/aog.2024.25 Published online by Cambridge University Press

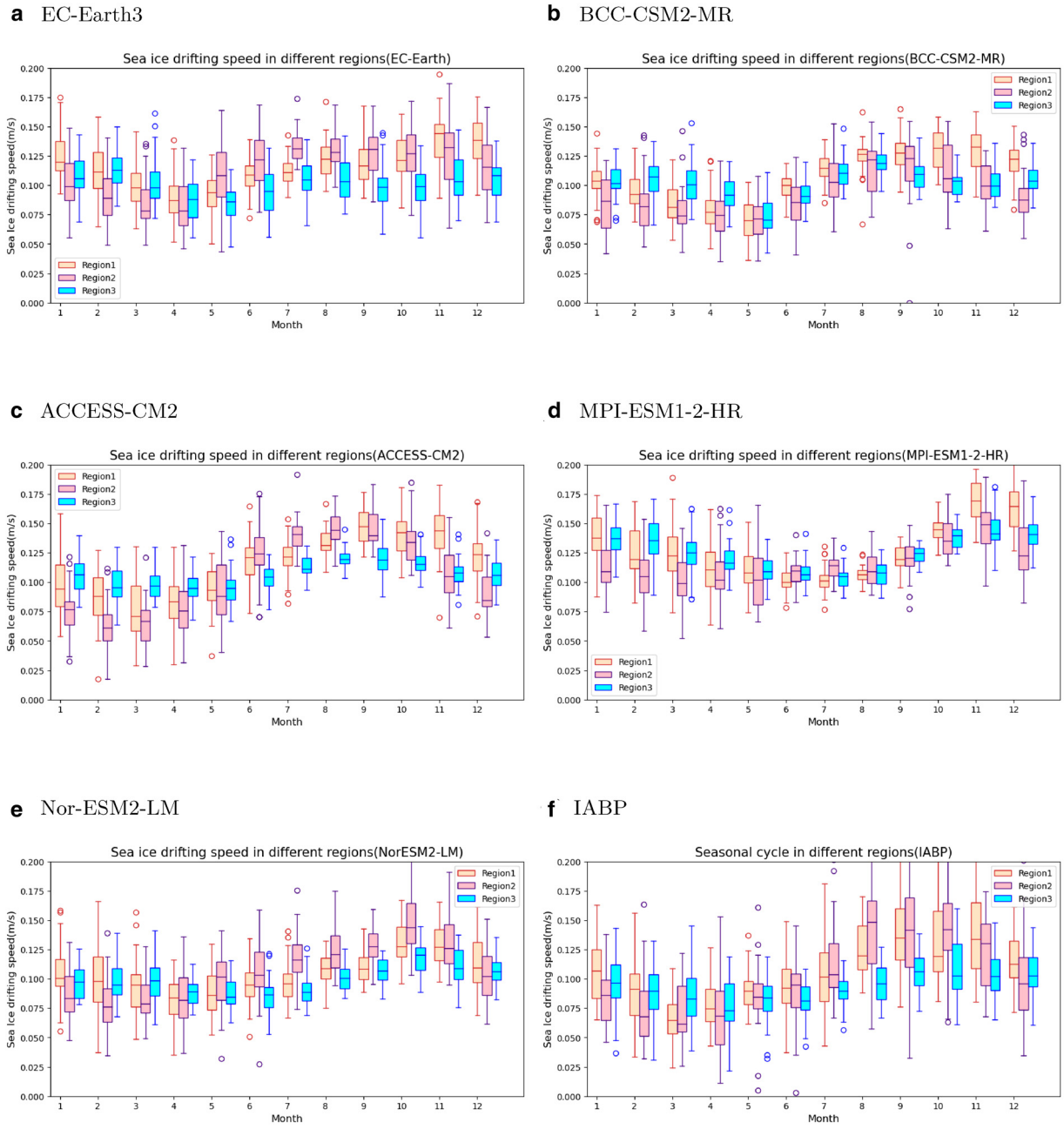

Figure 16. Regional comparison of sea ice motion between 1979 and 2014, incorporating both five CMIP6 models (a) EC-Earth3, (b) BCC-CSM2-MR, (c) ACCESS-CM2, (d) MPI-ESM1-2-HR, and (e) NorESM2-LM and (f) IABP data. Red boxes represent region 1, pink boxes represent region 2 and blue boxes represent region 3.

Figure 19 shows the relationship between sea ice thickness and sea ice motion in April and October based on PIOMAS-IABP data, PIOMAS-PIOMAS data and CMIP6 model data. The observation datasets, as well as all but one of the models, show a negative correlation between sea ice thickness and motion. The exception is the MPI-ESM1-2-HR model, which shows a very small positive correlation in October.

Table 3 shows the correlation coefficient and according p-value in Fig. 19. When the p-value is smaller than 0.05, the correlation between sea ice thickness and sea ice speed is significant. In April, the PIOMAS-IABP linear regression and PIOMAS-PIOMAS linear regression show insignificant negative slope while all models except ACCESS-CM2 exhibit a significant negative relationship. In October, there is a significant negative relationship between sea ice thickness and motion in PIOMAS-IABP, stronger than in April, while there is an insignificant and weak negative slope in the PIOMAS-PIOMAS correlation. All models except MPI-ESM1-2-HR simulate significant negative correlations, comparable with the PIOMAS-IABP result. The insignificant positive correlation which MPI-ESM1-2-HR shows between SIT and SISPEED is likely due to model deviation when simulating SISPEED.

Discussion and conclusion

We conduct validation of the selected CMIP6 models by comparing sea ice extent, thickness, and motion against buoy, satellite, and validated model data. We compare magnitudes, seasonal cycles and evolution trends. In addition, we analyze the dependence of ice motion on ice thickness.

The models generally simulate the seasonal cycle of sea ice extent well, except for EC-Earth3, where the minimum SIE occurs in August, rather than September as observed. The same discrepancy was highlighted in a study by Doscher and others (2021),

https://doi.org/10.1017/aog.2024.25 Published online by Cambridge University Press

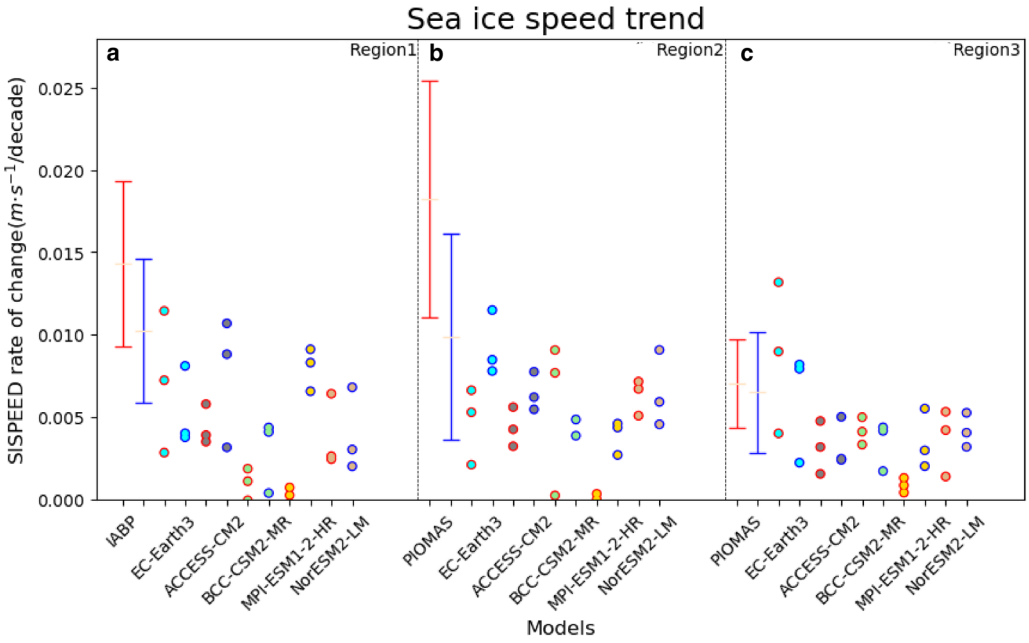

Figure 17. Trends of sea ice speed in IABP and five CMIP6 models (three ensemble for each model) between 1979 and 2014 with a unit of m/decade in (a) region 1, (b) region 2, and (c) region 3 in both summer and winter. IABP SISPEED trends are represented by error bars, red bars mean the range of summer SISPEED trend,blue bars mean the range of winter SISPEED trend. Model trends are represented by scatter plots. The red edge color represents modeled SISPEED trend in summer months, the blue edge color represents modeled SISPEED trend in winter months, and the different face colors of the boxes represent different CMIP6 models, denoted by *x*-axis.

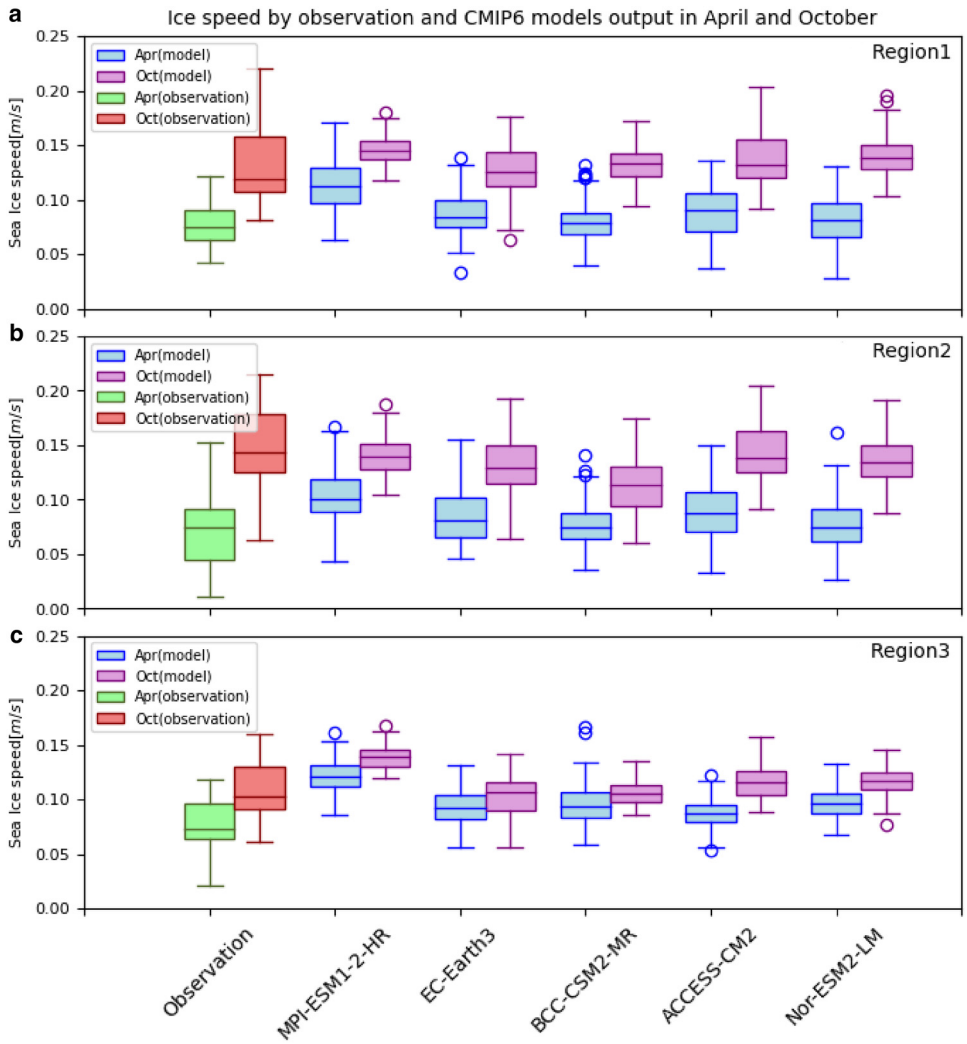

Figure 18. Comparison of sea ice motion between five selected CMIP6 models and observation in April and October in (a) Region 1, (b) Region 2, (c) Region 3, green boxes represent IABP data derived sea ice seed in April, red box represent IABP data derived sea ice seed in October, blue boxes represent selected CMIP6 models derived sea ice speed in April, and red boxes represent selected CMIP6 models derived sea ice speed in October.

https://doi.org/10.1017/aog.2024.25 Published online by Cambridge University Press

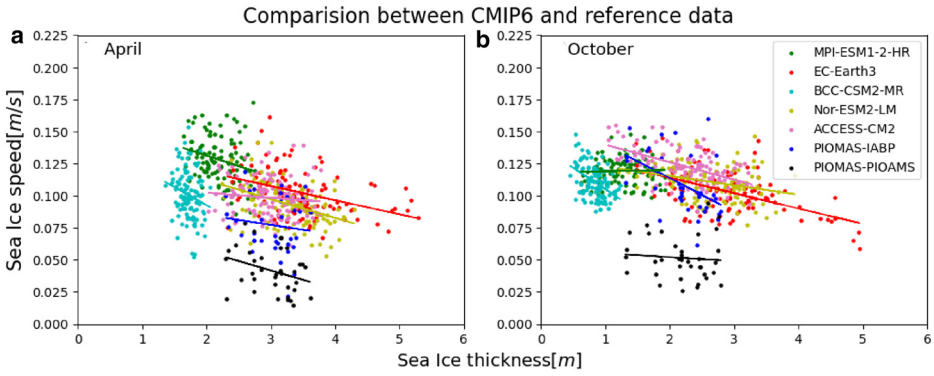

Figure 19. Correlation between sea ice motion and sea ice thickness in (a) April and (b) October in Central Arctic within reference data and with in each selected model using times series in 1979–2014, for reference data there are 36 data points whilst for modeled data there are 108 data points – since three ensemble members of each model are used. Reference data are PIOMAS-IABP SIT-SIM and PIOMAS-PIOMAS SIT-SIM.

NEMO-LIM3 models (ocean and sea-ice model components in EC-Earth3) demonstrated an August minimum SIA and overestimated SIV in March and September. The reason for this shift in timing might be the cold bias in EC-Earth, which leads to earlier freezing of the ocean (Palmeiro and others, 2023).

Doscher and others (2021) suggested that EC-Earth3 captured sea ice area rather well in March and September. In our results, the magnitude of SIE from EC-Earth3 simulations also agrees well with satellite data, despite the aforementioned shift in timing. The ACCESS-CM2 model simulates SIE greater than the reference data, especially in spring, while the BCC-CSM2-MR, MPI-ESM1-2-HR and Nor-ESM2-LM models underestimate SIE for most months. Satellite based SIE falls within the spread of CMIP6 output all year-round. Serreze and Stroeve (2015) examined satellite records and observed a strengthening of the decreasing trend in September SIE, associated with the positive ice-albedo feedback. Shu and others (2020) studied CMIP6 simulations of SIE in the Arctic and Antarctic and showed that CMIP6 slightly underestimates sea ice loss in September. We find that the simulated SIE trend in EC-Earth3 is comparable with the observed trend, while other CMIP6 models slightly underestimate the decreasing trend of SIE. This result agrees with (Shu and others, 2020).

There are ice-edge errors and uncertainties in PIOMAS SIT, especially in summer. PIOMAS and the NAOSIM model overestimate the thickness of thin ice and underestimate the thickness of thick ice, so that spatial variation is underestimated (Wang and others, 2016). Watts and others (2021) identified large ice-edge errors and ice thickness errors in CMIP6 models, but Watts and others (2021) showed that CMIP6 performed very well in simulating the magnitude, seasonal cycle, and trend of mean sea ice volume. The CMIP6 model output had a high spread in SIT and SIV (sea ice volume) for their study, and we also find a large spread in our results.

Our own CMIP6 model selection is based on the analysis of model performance in Notz and SIMIP community (2020).

Table 3. Correlation coefficient of the linear fit line describing the relation between sea ice thickness and sea ice speed in April and October in five CMIP6 models, in PIOMAS-IABP and in PIOMAS-PIOMAS, and according *p*-value

	April		October	
Model	*r*-value	*p*-value	*r*-value	*p*-value
MPI-ESM1-2-HR	−0.26	0.01	0.03	0.76
EC-Earth3	−0.39	0.00	−0.52	0.00
BCC-CSM2-MR	−0.20	0.04	−0.45	0.00
NorESM2-LM	−0.42	0.00	−0.30	0.00
ACCESS-CM2	−0.10	0.30	−0.56	0.00
PIOMAS-IABP	−0.13	0.45	−0.49	0.00
PIOMAS-PIOMAS	−0.32	0.06	−0.08	0.64

Keen and others (2021) showed that NorESM-LM and EC-Earth3 have a larger sea ice mass in the Arctic than PIOMAS, and EC-Earth3 undergoes more rapid ice loss over the historical period. This coincides with our assessment of SIT for these two models. Chen and others (2023) concluded that most CMIP6 models simulate SIT seasonal cycles well. Our own seasonal cycle analysis demonstrated that, based on PIOMAS, the maximum in mean SIT occurs in April (region1) or May (region2, 3) whilst the minimum SIT occurs in September(region 2, 3) or October(region 1). Most CMIP6 models simulate the seasonal cycle well, except EC-Earth3 and NorESM2-LM, which both exhibit phase-lags in the seasonal cycle. The SIT output from PIOMAS lies within the spread of CMIP6 model outputs. Three models have months when they overestimate ice thickness (EC-Earth3, ACCESS-CM2 and NorESM2-LM), while two models underestimate sea ice thickness (BCC-CSM2-MR, MPI-ESM1-2-HR). Models show substantial discrepancies in the melting season, with those models that overestimate SIT exhibiting even higher deviations in summer. Sun and Solomon (2021) noted the high initial state for SIT used in CICE, which leads to elevated SIT in the simulation results. ACCESS-CM2 and NorESM2-LM also use the CICE sea ice model component. This may account for their overestimation of SIT, aligning with the SIT validation findings in Xu and Li (2023). Notz and SIMIP community (2020) discussed that, CMIP6 models were insufficiently sensitive to warming in September, which could explain the high deviation from reference data in summer months. The variation between model simulations may in part be due to resolution and partly due to sea ice model components (Chen and others, 2023). Results from PIOMAS show faster sea ice thinning in summer than in winter, which is captured by most CMIP6 models. The sea ice thinning phenomenon is consistent across different Arctic regions, and the decreasing SIT trend in winter is captured well by models.

Most of the selected CMIP6 models show a slight lag of 1-2 months in simulating the seasonal cycle of sea ice motion, and thus they are in an acceptable range. MPI-ESM1-2-HR is an exception, as it fails to simulate the seasonal cycle of sea ice motion. Models simulate smaller seasonal cycle amplitudes compared to reference data, which leads to discrepancies in the magnitude of sea ice motion. Regarding the magnitude of sea ice motion, models perform better in the ice melting season than in the growing season. In the coastal Arctic seas, sea ice motion is much faster in summer than in winter, while in the central Arctic the seasonal variation of SIM is small. This phenomenon is captured by CMIP6 models with an exception of MPI-ESM1-2-HR. In general, the models overestimate motion in the first half of the year and underestimate motion in the second half of the year for coastal Arctic seas, while consistently overestimating sea ice motion in the central Arctic. The overestimation of sea ice speed in the central Arctic is similar to the

https://doi.org/10.1017/aog.2024.25 Published online by Cambridge University Press

behavior shown by Yu and others (2019) for the HIRHAM-NAOSIM model. The NorESM2-LM model provides the best simulation of sea ice motion among the selected CMIP6 models.

There is an Arctic-wide increasing trend in sea ice motion which is consistent between the selected CMIP6 models and IABP data. The latter shows that Region 2 (Laptev and East Siberian Seas) is undergoing the fastest rate of increase, followed by Region 1 (Beaufort and Chukchi Seas), while the Central Arctic is undergoing the slowest rate of increase. Zhang and others (2022) found a pattern of faster sea ice motion in the peripheral Arctic, based on satellite-derived data from NSIDC, which corresponds with IABP results. However, our selected models do not capture the different increasing trends across different Arctic regions, and simulate much lower increasing trends overall. In IABP data, the summer months tend to show a more rapid rate of increase in mean sea ice motion across the peripheral seas. Rampal and others (2009) and Zhang and others (2022) demonstrated that CMIP3 exhibits a greater increasing trend in sea ice motion during the cold season than in the warm season. From our analysis, most of the CMIP6 models simulate a higher rate of increase in the winter than in summer, which agrees with CMIP3, but is a contrast to IABP data.

SIT is one of the factors influencing sea ice motion variability. Sea ice thickness and sea ice motion magnitudes and trends are negative correlated in the reference data, with significant negative correlations in sea ice melting season (October) and insignificant negative correlations in April. This agrees with the argument of Rampal and others (2009) that there exists a positive feedback loop between increasing drift speed and thinning of sea ice. The coupling between sea ice state and sea ice motion is weak in April in CMIP6, consistent with previous results in CMIP3 and CMIP5 (Rampal and others, 2011).

Sea ice thermodynamic and dynamic processes are linked in a complex way, and the correlation between SIE, SIT, and sea ice motion may be nonlinear. For example, the divergence of sea ice could drive different tendencies in sea ice growth or melt depending on the season (Notz and SIMIP Community, 2020). We observe a systematic error in CMIP6 model simulations: as an example, EC-Earth3 and ACCESS-CM2 models tend to overestimate SIE and SIT, but they also overestimate sea ice motion. Similarly, the BCC-CSM2-MR model tends to underestimate SIE, SIT and sea ice motion in the marginal seas. This contrasts with the prevailing assumption that overestimation of sea ice volume should be associated with underestimation of sea ice motion.

The goal of our study is to fill the gap in validation of the sea ice motion fields produced by CMIP6 models. This complements previous model validation studies focused on SIE and SIT. Our assessment of different regions when evaluating CMIP6 models helps to identify shortcomings in the simulations across different locations and environments. Similarly, by separating the trends between different seasons, we demonstrate that CMIP6 simulations of ice loss and ice motion undergo increasing trends which remain overly conservative in the summer months. This is a feature of CMIP6 model performance which could be improved in the future. Furthermore, the analysis linking SIT and SIE with sea ice motion indicates a correlated, yet nonlinear relationship, suggesting that other factors impacting sea ice motion evolution need further study.

CMIP6 models demonstrate improvement compared to CMIP3 and CMIP5 models Stroeve and others (2012). The decreasing trend of sea ice loss is closer to observations, and they are less conservative when simulating ice loss (Shu and others, 2020). However our study shows that a majority of CMIP6 models still exhibit a conservative bias in the rate of decrease for both SIE and SIT. CMIP6 models simulate the seasonal cycle of SIE well, but for SIT and sea ice motion some models exhibit shifted seasonal cycles. The MPI-ESM1-2-HR model in particular struggles to reproduce the observed sea ice motion. The selected CMIP6 models fail to capture the variety in sea ice trends across different regions and seasons. In particular the increasing trend in sea ice thinning and in sea ice motion observed in the coastal Arctic seas is underestimated by the models, especially in the Laptev and East Siberian Seas during summer months. In the future, model development should place more emphasis on the summer and on the simulation of the marginal ice zone in order to improve the robustness of results.

Acknowledgements. We are grateful for Istvan Heiler on processing the IABP data for this study. We are also thankful to Andrew Twelves for his meticulous proofreading of the English. This project has received funding from the European Union's Horizon 2020 research and innovation program under grant agreement No 101003826 via project CRiceS (Climate Relevant interactions and feedbacks: the key role of sea ice and Snow in the polar and global climate system).

Author contributions. XZ conducted the data analysis and drafted the manuscript. JH and PU contributed to interpretation and writing of the manuscript. JH defined the research objectives and designed the study.

References

Bi D and 9 others (2020) Configuration and spin-up of access-cm2, the new generation australian community climate and earth system simulator coupled model. *Journal of Southern Hemisphere Earth Systems Science* **70**(1), 225–251.

Bitz CM, Holland MM, Weaver AJ and Eby M (2001) Simulating the ice-thickness distribution in a coupled climate model. *Journal of Geophysical Research: Oceans* **106**(C2), 2441–2463. doi: 10.1029/1999JC000113

Chen L and 5 others (2023) The Arctic sea ice thickness change in CMIP6's historical simulations. *Advances in Atmospheric Sciences* **40**, 1–13. doi: 10.1007/s00376-022-1460-4

Chevallier M and Salas y Melia D (2011) The impact of the inclusion of new sea ice processes on the simulation of Arctic sea ice in cnrm-cm coupled model. *AGU Fall Meeting Abstracts* 0544.

Crawford AD, Rosenblum E, Lukovich JV and Stroeve JC (2023) Sources of seasonal sea-ice bias for cmip6 models in the Hudson Bay Complex. *Annals of Glaciology* 1–18. doi: 10.1017/aog.2023.42

Dix M and 33 others (2019) Csiro-arccss access-cm2 model output prepared for cmip6 cmip historical. doi: 10.22033/ESGF/CMIP6.4271

Docquier D and 5 others (2017) Relationships between Arctic sea ice drift and strength modelled by nemo-lim3.6. *The Cryosphere* **11**(6), 2829–2846. doi: 10.5194/tc-11-2829-2017

Doscher R and 9 others (2021) The ec-earth3 earth system model for the climate model intercomparison project 6. *Geoscientific Model Development Discussions* **2021**, 1–90.

Doscher R and 60 others (2022) The ec-earth3 earth system model for the coupled model intercomparison project 6. *Geoscientific Model Development* **15**(7), 2973–3020. doi: 10.5194/gmd-15-2973-2022

ESGF (2022) *Earth System Grid Federation*. ESGF. https://aims2.llnl.gov/search/cmip6/

Gerland S and 9 others (2019) Essential gaps and uncertainties in the understanding of the roles and functions of Arctic sea ice. *Environmental Research Letters* **14**(4), 043002.

Hibler WD (1979) A dynamic thermodynamic sea ice model. *Journal of Physical Oceanography* **9**(4), 815–846. doi: 10.1175/1520-0485(1979)009<0815:ADTSIM>2.0.CO;2

Hunke E and Lipscomb W (2010) *Cice: the los alamos sea ice model documentation and software user's manual version 4.0 la-cc-06-012*. Tech. Rep. LA-CC-06-012. Los Alamos, NM: Los Alamos National Laboratory.

Hunke EC and Comeau D (2011) Sea ice and iceberg dynamic interaction. *Journal of Geophysical Research: Oceans* **116**(C5), C05008. doi: 10.1029/2010JC006588

Jungclaus J and 47 others (2019) Mpi-m mpi-esm1.2-hr model output prepared for cmip6 cmip historical. doi: 10.22033/ESGF/CMIP6.6594

Keen A and 17 others (2021) An inter-comparison of the mass budget of the Arctic sea ice in cmip6 models. *The Cryosphere* **15**(2), 951–982. doi: 10.5194/tc-15-951-2021

Kern S and 6 others (2019) Satellite passive microwave sea-ice concentration data set intercomparison: closed ice and ship-based observations. *The Cryosphere* **13**(12), 3261–3307.

Kirchner J (2001) *Data Analysis Toolkit# 5: Uncertainty Analysis and Error Propagation*. University of California Berkeley Seismological Laboratory. Available at: http://seismo.berkeley.edu/kirchner/eps_120/Toolkits/Toolkit_05.pdf

Kwok R, Spreen G and Pang S (2013) Arctic sea ice circulation and drift speed: decadal trends and ocean currents. *Journal of Geophysical Research: Oceans* **118**(5), 2408–2425. doi: 10.1002/jgrc.20191

Lee YJ, Watts M, Maslowski W, Kinney JC and Osinski R (2023) Assessment of the pan-Arctic accelerated rate of sea ice decline in cmip6 historical simulations. *Journal of Climate* **36**(17), 6069–6089.

Leppäranta M (2010) *The Drift of Sea Ice*. Springer Science & Business Media.

Mackie S and 5 others (2020) Sea ice formation in a coupled climate model including grease ice. *Journal of Advances in Modeling Earth Systems* **12**(8), e2020MS002103. doi: 10.1029/2020MS002103

Maeda K, Kimura N and Yamaguchi H (2020) Temporal and spatial change in the relationship between sea-ice motion and wind in the Arctic. *Polar Research* **39**, 3370. doi: 10.33265/polar.v39.3370

Mauritsen T and 68 others (2019) Developments in the mpi-m earth system model version 1.2 (mpi-esm1.2) and its response to increasing CO2. *Journal of Advances in Modeling Earth Systems* **11**(4), 998–1038. doi: 10.1029/2018MS001400

Notz D and SIMIP Community (2020) Arctic sea ice in cmip6. *Geophysical Research Letters* **47**(10), e2019GL086749. doi: 10.1029/2019GL086749

Oikkonen A and Haapala J (2011) Variability and changes of Arctic sea ice draft distribution – submarine sonar measurements revisited. *The Cryosphere* **5**(4), 917–929. doi: 10.5194/tc-5-917-2011

Olason E and Notz D (2014) Drivers of variability in Arctic sea-ice drift speed. *Journal of Geophysical Research: Oceans* **119**(9), 5755–5775. doi: 10.1002/2014JC009897

Palmeiro FM and 5 others (2023) Boreal winter stratospheric climatology in ec-earth: cmip6 version. *Climate Dynamics* **60**(3-4), 883–898.

Parodi-Perdomo JA (2019) Ec-earth-consortium ec-earth3 model output prepared for cmip6 cmip historical. doi: 10.22033/ESGF/CMIP6.4700

Rampal P, Weiss J and Marsan D (2009) Positive trend in the mean speed and deformation rate of Arctic sea ice, 1979–2007. *Journal of Geophysical Research: Oceans* **114**(C5), C05013.

Rampal P, Weiss J, Dubois C and Campin JM (2011) Ipcc climate models do not capture Arctic sea ice drift acceleration: consequences in terms of projected sea ice thinning and decline. *Journal of Geophysical Research: Oceans* **116**(C8), C00D07. doi: 10.1029/2011JC007110

Rigor I (2017) *IABP drifting buoy pressure, temperature, position, and interpolated ice velocity, version 1* (g00791). IABP.

Rigor IG, Wallace JM and Colony RL (2002) Response of sea ice to the Arctic oscillation. *Journal of Climate* **15**(18), 2648–2663.

Rind D, Perlwitz J, Lonergan P and Lerner J (2005) Ao/nao response to climate change: 2. relative importance of low- and high-latitude temperature changes. *Journal of Geophysical Research: Atmospheres* **110**(D12), D12108. doi: 10.1029/2004JD005686

Schroeter S, Hobbs W, Bindoff NL, Massom R and Matear R (2018) Drivers of Antarctic sea ice volume change in cmip5 models. *Journal of Geophysical Research: Oceans* **123**(11), 7914–7938. doi: 10.1029/2018JC014177

Schweiger (2011) Uncertainty in modeled Arctic sea ice volume. doi: 10.1029/2011JC007084

Seland O and 9 others (2020) Overview of the Norwegian Earth System Model (NorESM2) and key climate response of CMIP6 DECK, historical, and scenario simulations. *Geoscientific Model Development* **13**(12), 6165–6200.

Seland y, Bentsen M and 28 others (2019) Ncc noresm2-lm model output prepared for cmip6 cmip historical. doi: 10.22033/ESGF/CMIP6.8036

Semtner Jr. AJ (1976) A model for the thermodynamic growth of sea ice in numerical investigations of climate. *Journal of Physical Oceanography* **6**(3), 379–389.

Serreze M and Stroeve J (2015) Arctic sea ice trends, variability and implications for seasonal ice forecasting. *Philosophical Transactions Series A, Mathematical, Physical, and Engineering Sciences* **373**, 0159. doi: 10.1098/rsta.2014.0159

Shu Q and 6 others (2020) Assessment of sea ice extent in cmip6 with comparison to observations and cmip5. *Geophysical Research Letters* **47**(9), e2020GL087965. doi: 10.1029/2020GL087965

Stroeve JC and 6 others (2012) Trends in Arctic sea ice extent from CMIP5, CMIP3 and observations. *Geophysical Research Letters* **39**(16), L16502. doi: 10.1029/2012GL052676

Sumata H, de Steur L, Divine DV, Granskog MA and Gerland S (2023) Regime shift in Arctic ocean sea ice thickness. *Nature* **615**(7952), 443–449.

Sun S and Solomon A (2021) Seasonal sea ice prediction with the cice model and positive impact of cryosat-2 ice thickness initialization. *The Cryosphere Discussions* 1–18.

Theil H (1992) *A Rank-Invariant Method of Linear and Polynomial Regression Analysis*. Dordrecht: Springer Netherlands. pp. 345–381.

Thomas D (1999) The quality of sea ice velocity estimates. *Journal of Geophysical Research: Oceans* **104**(C6), 13627–13652. doi: 10.1029/1999JC900086

Thorndike AS, Rothrock DA, Maykut GA and Colony R (1975) The thickness distribution of sea ice. *Journal of Geophysical Research (1896-1977)* **80**(33), 4501–4513. doi: 10.1029/JC080i033p04501

Uotila P, O'Farrell S, Marsland S and Bi D (2013) The sea-ice performance of the australian climate models participating in the cmip5. *Australian Meteorological and Oceanographic Journal* **63**(1), 121–143.

Vancoppenolle M and 5 others (2009) Simulating the mass balance and salinity of Arctic and Antarctic sea ice. 1. model description and validation. *Ocean Modelling* **27**(1), 33–53. doi: 10.1016/j.ocemod.2008.10.005

Voldoire A and 9 others (2013) The cnrm-cm5. 1 global climate model: description and basic evaluation. *Climate Dynamics* **40**, 2091–2121.

Walsh JE, Fetterer F, Stewart JS and Chapman WL (2017) A database for depicting Arctic sea ice variations back to 1850. *Geographical Review* **107**(1), 89–107. doi: 10.1111/j.1931-0846.2016.12195.x

Wang X, Key J, Kwok R and Zhang J (2016) Comparison of Arctic sea ice thickness from satellites, aircraft, and piomas data. *Remote Sensing* **8**(9), 713. doi: 10.3390/rs8090713

Watts M, Maslowski W, Lee YJ, Kinney JC and Osinski R (2021) A spatial evaluation of Arctic sea ice and regional limitations in cmip6 historical simulations. *Journal of Climate* **34**(15), 6399–6420. doi: 10.1175/JCLI-D-20-0491.1

Wu T and 14 others (2018) Bcc-csm2-mr model output prepared for cmip6 cmip historical. doi: 10.22033/ESGF/CMIP6.2948

Xu M and Li J (2023) Assessment of sea ice thickness simulations in the cmip6 models with cice components. *Frontiers in Marine Science* **10**, 1223772.

Yu X and 6 others (2019) Evaluation of Arctic sea-ice drift and its dependency on near-surface wind and sea-ice concentration and thickness in the coupled regional climate model HIRHAM–NAOSIM. *The Cryosphere Discussions* **14**(5), 1727–1746. doi: 10.5194/tc-2019-183

Zdaniuk B (2014) *Ordinary Least-Squares (OLS) Model*. Dordrecht: Springer Netherlands, pp. 4515–4517.

Zhang F and 5 others (2022) Arctic sea ice motion change and response to atmospheric forcing between 1979 and 2019. *International Journal of Climatology* **42**(3), 1854–1876. doi: 10.1002/joc.7340

https://doi.org/10.1017/aog.2024.25 Published online by Cambridge University Press

Appendix

Table 4. Deviation(%) of sea ice extent in five selected CMIP6 models EC-Earth3, ACCESS-CM2, BCC-CSM2-MR, MPI-ESM1-2-HR and NorESM2-LM compared with satellite derived SIE, observation and CMIP6 model output is represented by the mean value of sea ice extent between 1979 and 2014 in each month

	Jan	Feb	Mar	Apr	May	Jun	Jul	Aug	Sep	Oct	Nov	Dec
EC-Earth3	3 ± 8	1 ± 7	1 ± 7	3 ± 8	5 ± 8	1 ± 9	−6 ± 18	−4 ± 26	12 ± 44	10 ± 26	7 ± 13	5 ± 19
ACCECC-CM2	2 ± 8	4 ± 7	6 ± 7	11 ± 8	15 ± 8	10 ± 10	5 ± 21	3 ± 28	6 ± 42	3 ± 25	0 ± 12	0 ± 8
BCC-CSM2-MR	−11 ± 7	−11 ± −6	−10 ± 6	−9 ± 7	−11 ± 6	−15 ± 7	−18 ± 16	−26 ± 20	−23 ± 30	−18 ± 20	−17 ± 10	−12 ± 7
MPI-ESM1-2-HR	−4 ± 7	−5 ± 6	−3 ± 6	−1 ± 7	2 ± 7	−2 ± 9	−13 ± 17	−14 ± 23	−7 ± 36	−12 ± 21	−8 ± 11	−7 ± 8
NorESM2-LM	−5 ± 7	−7 ± 6	−7 ± 6	−6 ± 7	−4 ± 7	−5 ± 8	−4 ± 19	2 ± 28	8 ± 43	7 ± 26	0 ± 12	−2 ± 8

Deviation within ±2σ were considered plausible. Red color means model overestimates, blue color means model underestimates.

Table 5. Deviation (%) and uncertainties accosiated with the deviation (%) of sea ice thickness in (a) region 1, (b) region 2, and (c) region 3 in five CMIP6 models: EC-Earth3, ACCESS-CM2, BCC-CSM2-MR, MPI-ESM1-2-HR, and NorESM2-LM compared with PIOMAS data

	Jan	Feb	Mar	Apr	May	Jun	Jul	Aug	Sep	Oct	Nov	Dec
(a) Region 1												
EC-Earth3	27 ± 88	23 ± 78	24 ± 76	25 ± 76	29 ± 83	40 ± 96	69 ± 148	60 ± 226	48 ± 240	48 ± 209	62 ± 165	40 ± 110
ACCESS-CM2	27 ± 92	23 ± 79	21 ± 76	20 ± 74	22 ± 78	28 ± 88	41 ± 129	18 ± 153	17 ± 175	21 ± 160	47 ± 148	33 ± 119
BCC-CSM2-MR	−47 ± 33	−44 ± 30	−43 ± 34	−41 ± 37	−40 ± 39	−45 ± 42	−51 ± 56	−60	−68	−71	−66	−55 ± 33
MPI-ESM1-2-HR	−17 ± 58	−13 ± 52	−12 ± 53	−11 ± 55	−12 ± 55	−16 ± 58	−32 ± 61	−39	−38	−41 ± 75	−24 ± 75	−21 ± 66
NorESM2-LM	20 ± 96	11 ± 82	9 ± 78	8 ± 76	11 ± 78	24 ± 90	40 ± 126	31 ± 187	28 ± 201	39 ± 203	46 ± 161	33 ± 118
(b) Region 2												
EC-Earth3	54 ± 154	52 ± 134	51 ± 121	49 ± 125	45 ± 122	58 ± 133	93 ± 190	179	228	133	103 ± 277	63 ± 196
ACCESS-CM2	48 ± 129	43 ± 107	41 ± 96	39 ± 101	40 ± 110	50 ± 135	66 ± 169	123	175	113	99 ± 282	55 ± 172
BCC-CSM2-MR	−20 ± 62	−20 ± 54	−20 ± 50	−22 ± 53	−21 ± 62	−22 ± 66	−28	−26	−26	−34	−34	−19 ± 80
MPI-ESM1-2-HR	−2 ± 80	2 ± 73	4 ± 67	3 ± 72	1 ± 75	−7 ± 77	−20	−18	−17	−15	−22	−6 ± 97
NorESM2-LM	25 ± 135	23 ± 115	20 ± 100	17 ± 101	17 ± 110	25 ± 127	50 ± 158	113	163	73	24	29 ± 170
(c) Region 3												
EC-Earth3	32 ± 85	28 ± 79	24 ± 72	22 ± 67	23 ± 65	28 ± 71	42 ± 98	49 ± 128	42 ± 127	41 ± 120	41 ± 108	37 ± 96
ACCESS-CM2	5 ± 69	4 ± 63	3 ± 58	2 ± 54	5 ± 53	10 ± 58	14 ± 78	16 ± 103	10 ± 106	9 ± 97	12 ± 91	7 ± 78
BCC-CSM2-MR	−43 ± 29	−40 ± 28	−38 ± 28	−37 ± 27	−37 ± 26	−36 ± 29	−37 ± 39	−42 ± 42	−48 ± 46	−51 ± 38	−49 ± 33	−47 ± 30
MPI-ESM1-2-HR	−27 ± 43	−25 ± 40	−24 ± 38	−23 ± 36	−24 ± 34	−27 ± 35	−35 ± 41	−46 ± 45	−47 ± 47	−38 ± 47	−31 ± 51	−29 ± 47
NorESM2-LM	24 ± 83	20 ± 76	18 ± 70	17 ± 66	17 ± 65	21 ± 72	34 ± 100	40 ± 135	36 ± 144	34 ± 130	36 ± 109	29 ± 95

PIOMAS and CMIP6 model output (sivol) is represented by the mean value of sea ice thickness between 1979–2014 in each month. Data points lower than 0.5 m are excluded to minimize edge effects. Deviation within ±2σ were considered plausible. Red color means model overestimates, blue color means model underestimates.

Table 6. Deviation (%) along with the uncertainties accociated with the deviation in percentage of sea ice motion in (a) region 1 (b) region 2 (c) region 3 in five selected CMIP6 models: EC-Earth3, ACCESS-CM2, BCC-CSM2-MR, MPI-ESM1-2-HR and NorESM2-LM when comparing with IABP derived sea ice motion. Observation and CMIP6 model output is represented by the mean value of sea ice motion between 1979–2014 in each month

	Jan	Feb	Mar	Apr	May	Jun	Jul	Aug	Sep	Oct	Nov	Dec
(a) Region 1												
EC-Earth3	15 ± 154	24 ± 177	44 ± 224	16 ± 168	−1 ± 112	11 ± 118	10 ± 130	−1 ± 99	−8 ± 101	−2 ± 120	1 ± 133	10 ± 166
ACCESS-CM2	−8 ± 125	−2 ± 143	15 ± 188	11 ± 159	9 ± 126	24 ± 133	14 ± 137	4 ± 106	4 ± 114	7 ± 131	4 ± 135	−1 ± 146
BCC-CSM2-MR	−2 ± 129	8 ± 154	32 ± 211	6 ± 155	−16 ± 96	3 ± 116	9 ± 138	−1 ± 111	−7 ± 116	4 ± 131	−1 ± 126	0 ± 146
MPI-ESM1-2-HR	31 ± 170	47 ± 206	83 ± 289	52 ± 212	27 ± 140	9 ± 113	−1 ± 115	−19 ± 82	−19 ± 88	8 ± 125	25 ± 155	34 ± 194
NorESM2-LM	0 ± 139	10 ± 161	35 ± 212	18 ± 171	2 ± 117	2 ± 112	−4 ± 116	−16 ± 87	−19 ± 87	−7 ± 112	−3 ± 127	−2 ± 146
(b) Region 2												
EC-Earth3	21 ± 143	34 ± 158	46 ± 202	43 ± 208	24 ± 490	17 ± 122	−7 ± 118	−26 ± 88	−25 ± 83	−28 ± 89	−15 ± 119	4 ± 145
ACCESS-CM2	−12 ± 103	−2 ± 127	6 ± 168	1 ± 152	−9 ± 667	−15 ± 120	−33 ± 136	−47 ± 97	−45 ± 89	−47 ± 94	−38 ± 99	−22 ± 119
BCC-CSM2-MR	−13 ± 106	−4 ± 140	−2 ± 169	−2 ± 142	−20 ± 448	−14 ± 88	−15 ± 93	−20 ± 87	−18 ± 75	−26 ± 81	−27 ± 88	−21 ± 118
MPI-ESM1-2-HR	29 ± 174	34 ± 161	39 ± 244	44 ± 182	22 ± 645	19 ± 91	−5 ± 95	−29 ± 72	−22 ± 73	−10 ± 91	11 ± 124	23 ± 179
NorESM2-LM	−5 ± 115	6 ± 125	15 ± 190	11 ± 185	−2 ± 759	−7 ± 99	−27 ± 105	−41 ± 79	−40 ± 79	−42 ± 93	−32 ± 116	−16 ± 137
(c) Region 3												
EC-Earth3	15 ± 173	26 ± 199	18 ± 192	20 ± 193	7 ± 150	18 ± 141	18 ± 126	13 ± 127	−3 ± 113	−6 ± 113	1 ± 135	0 ± 139
ACCESS-CM2	13 ± 170	16 ± 186	16 ± 193	28 ± 202	17 ± 167	27 ± 152	26 ± 137	26 ± 140	12 ± 130	4 ± 123	4 ± 137	4 ± 146
BCC-CSM2-MR	4 ± 159	14 ± 180	11 ± 175	17 ± 189	−10 ± 132	6 ± 130	17 ± 127	20 ± 133	−1 ± 116	−10 ± 110	−7 ± 122	−6 ± 130
MPI-ESM1-2-HR	42 ± 214	48 ± 235	43 ± 229	52 ± 237	34 ± 194	29 ± 155	12 ± 122	6 ± 121	7 ± 125	20 ± 143	30 ± 170	31 ± 181
NorESM2-LM	−3 ± 151	6 ± 175	7 ± 180	11 ± 181	4 ± 149	2 ± 127	−1 ± 110	0 ± 115	4 ± 121	3 ± 125	2 ± 141	−4 ± 138

Deviation within ±2σ were considered plausible. Red color means model overestimates, blue color means model underestimates.

https://doi.org/10.1017/aog.2024.25 Published online by Cambridge University Press